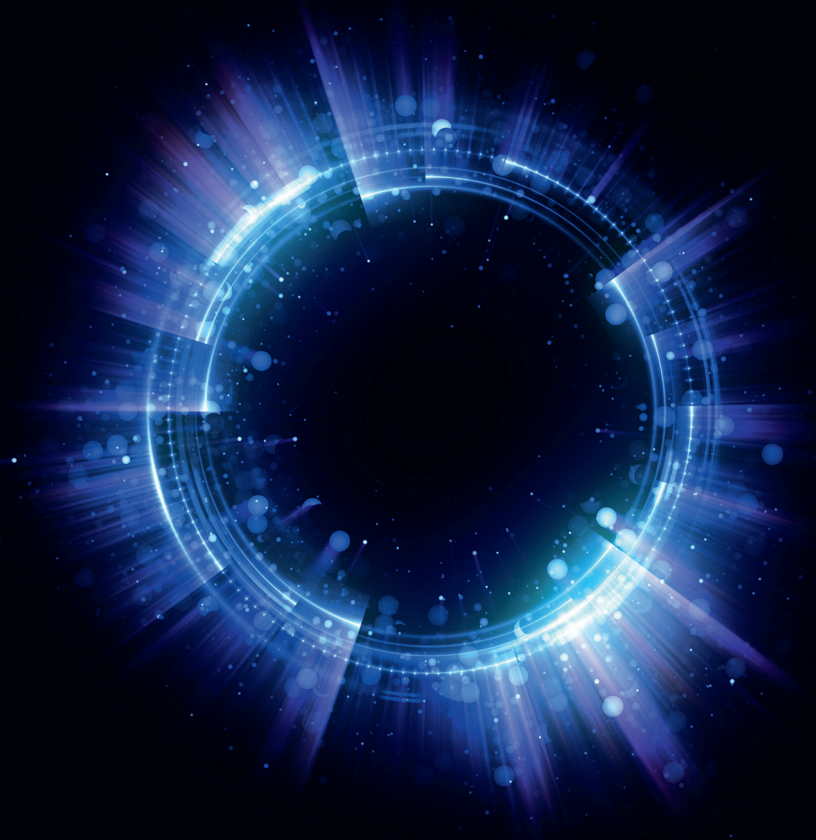


Rihards Mūrnieks

**FABRICATION OF WHISPERING GALLERY MODE
RESONATORS AND IMPLEMENTATION IN FIBRE
OPTICAL COMMUNICATION SYSTEMS**

Summary of the Doctoral Thesis



RIGA TECHNICAL UNIVERSITY

Faculty of Electronics and Telecommunications
Institute of Telecommunications

Rihards Mūrnieks

Doctoral Student of the Study Programme “Telecommunications”

**FABRICATION OF WHISPERING GALLERY
MODE RESONATORS AND IMPLEMENTATION
IN FIBRE OPTICAL COMMUNICATION
SYSTEMS**

Summary of the Doctoral Thesis

Scientific supervisor
Professor Dr. sc. ing. VJAČESLAVS BOBROVS
Professor Dr. sc. ing. JURĢIS PORIŅŠ

RTU Press
Riga, 2023

Mūrnieks, R. Fabrication of Whispering Gallery Mode Resonators and Implementation in Fibre Optical Communication Systems. Summary of the Thesis – Riga: RTU Press, 2023. – 52 p.

Published in accordance with the decision of the Promotion Council “RTU-P08” of 30 June 2023, Minutes No. 23.

The present Doctoral Thesis was developed with the support of the grant of the European Social Fund in the field of strategic specialization of strengthening the doctoral students and academic staff of the Riga Technical University and BA School of Business and Finance, grant No. 8.2.2.0/20/I/008.

**NATIONAL
DEVELOPMENT
PLAN 2020**



EUROPEAN UNION

European Regional
Development Fund

INVESTING IN YOUR FUTURE

<https://doi.org/10.7250/9789934229848>

ISBN 978-9934-22-984-8 (pdf)

DOCTORAL THESIS PROPOSED TO RIGA TECHNICAL UNIVERSITY FOR THE PROMOTION TO THE SCIENTIFIC DEGREE OF DOCTOR OF SCIENCE

To be granted the scientific degree of Doctor of Science (Ph. D.), the present Doctoral Thesis has been submitted for the defence at the open meeting of RTU Promotion Council on 17 November 2023 at the Faculty of Electronics and Telecommunications of Riga Technical University, 12 Āzenes Street, Room 201.

OFFICIAL REVIEWERS

Associate Professor Dr. sc. ing. Aleksandrs Ipatovs
Riga Technical University

Leading Researcher Ph. D. Oskars Java
Vidzeme University of Applied Sciences, Latvia

Associate Professor Francesco Da Ros
Technical University of Denmark, Denmark

DECLARATION OF ACADEMIC INTEGRITY

I hereby declare that the Doctoral Thesis submitted for review to Riga Technical University for promotion to the scientific degree of Doctor of Science (Ph. D.) is my own. I confirm that this Doctoral Thesis has not been submitted to any other university for promotion to a scientific degree.

Rihards Mūrnieks (signature)

Date:

The present Doctoral Thesis has been prepared as a set of thematically related scientific publications with a summary in Latvian and English. The Doctoral Thesis is written in the Latvian language. It contains an introduction, 3 chapters, conclusions, a bibliography (list of references), 38 figures, 5 tables, and 7 appendices; a total of 81 pages, excluding the appendices. The bibliography contains 167 titles. The Doctoral Thesis summarizes 7 of the author's 13 original scientific articles. Scientific publications are written in English and indexed in SCOPUS, IEEE and WoS database; their total number of pages is 77.

THE PRESENT DOCUMENT IS ELECTRONICALLY SIGNED WITH A SECURE ELECTRONIC SIGNATURE AND CONTAINS A TIME STAMP.

Acknowledgements

I express my appreciation and gratitude to the supervisors of the Thesis, Professor Vjačeslavs Bobrovs and Professor Jurgis Poriņš, and the Head of the Communication Systems Technology Research Centre of RTU ETF Institute of Telecommunications Professor Sandis Spolītis for the support and advice provided during the development of the Doctoral Thesis.

Being a researcher at the Institute of Telecommunications of RTU Faculty of Electronics and Telecommunications (ETF), I had the opportunity to work and collaborate with talented, professional, and supportive colleagues and fellow students. I express my gratitude to everyone for their support, teamwork, and knowledge, the lack of which would mean this Thesis could not exist. I express my special appreciation to the long-term colleagues Toms Salgals, Jānis Braunfelds, Armands Ostrovskis, and Laura Skladova.

I thank all the professors, assistant professors and lecturers who provided their knowledge in the long lectures, practical and laboratory work during my bachelor, master and doctoral studies. I express my deepest appreciation to other ETF and RTU employees who were always helpful and ready to assist. Also, thanks to my long-time assistant who spent many hours with me inside and outside the university.

Finally, the biggest and warmest thanks go to my beloved family – brothers, sisters, and especially my mother, without whose 24/7 support, faith and dedication I would not have reached this moment and completed the Thesis.

TABLE OF CONTENTS

GENERAL DESCRIPTION OF THE THESIS	7
Topic Introduction	7
Aim, Tasks and Theses to be Substantiated	8
Scientific Novelty and Main Results	8
Structure and Volume of the Thesis	9
Approbation of Thesis Results and Publications	9
INTRODUCTION	12
MAIN RESULTS OF THE THESIS	14
1. FABRICATION OF SILICA RESONATORS AND EVALUATION OF THEIR PARAMETERS AND OPTICAL CARRIER GENERATION FOR DATA TRANSMISSION	14
1.1. Description of Silica Microsphere Fabrication	14
1.2. Description of Silica Micro-rod Fabrication	15
1.3. Evaluation of Optical Frequency Comb Generation	17
2. ANALYSIS OF AN OPTICAL FREQUENCY COMB GENERATION IN MICROSPHERES AND MICRO-RODS CORRESPONDING TO FIBRE OPTICAL TRANSMISSION SYSTEM NEEDS	22
2.1. Generation of an Optical Frequency Comb in Silica Microsphere with 400-GHz FSR	22
2.2. Generation of a Dissipative Kerr Soliton Comb in Silica Resonator with 100-GHz FSR	23
2.3. Development of an Experimental Optical Frequency Comb Light Source Based on Silica Micro-rod with 90-GHz FSR	26
3. EVALUATION OF MICROSPHERE AND MICRO-ROD OPTICAL FREQUENCY COMB LIGHT SOURCE IMPLEMENTATION IN HIGH-SPEED DATA TRANSMISSION SYSTEMS	31
3.1. Development of the IM/DD 4-channel 200 GHz Spaced WDM-PON System Based on Microsphere OFC light source	31
3.2. Development of the IM/DD 4-Channel 400 GHz Spaced WDM-PON System Based on a Microsphere OFC Light Source with Different Optical Fibre Transmission Lines	33
3.3. Development of the IM/DD 8-Channel 100 GHz Spaced WDM-PON System Based on a Microsphere OFC Light Source with Different Optical Carrier Linewidth Values	36
3.4. Development of the Experimental 100 Gbit/s Data Centre Interconnect Based on a Micro-rod OFC Light Source	41
CONCLUSIONS	47
REFERENCES	48

List of Abbreviations

<i>ASE</i>	Amplified Spontaneous Emission	<i>NG-PON2</i>	40-Gigabit-Capable Passive Optical Network
<i>AWG-DEMUX</i>	Arrayed Waveguide Grating Multiplexer	<i>NRZ</i>	Non-Return-to Zero
<i>AWG-MUX</i>	Arrayed Waveguide Grating Demultiplexer	<i>NRZ-OOK</i>	Non-Return-to Zero On-Off Keying
<i>BER</i>	Bit-Error Rate	<i>NZ-DSF</i>	Non-Zero Dispersion-Shifted Fibre
<i>B2B</i>	Back-to-Back	<i>OBPF</i>	Optical Bandpass Filter
<i>CD</i>	Chromatic Dispersion	<i>OC</i>	Optical Circulator
<i>CFWM</i>	Cascaded Four-Wave Mixing	<i>ODN</i>	Optical Distribution Network
<i>CO</i>	Central Office	<i>OFC</i>	Optical Frequency Comb
<i>CSF</i>	Cut-off Shifted Fibre	<i>OLT</i>	Optical Line Terminal
<i>CW</i>	Continuous Wave	<i>ONT</i>	Optical Network Terminal
<i>DCI</i>	Data Centre Interconnect	<i>OSA</i>	Optical Spectrum Analyser
<i>DKS</i>	Dissipative Kerr Soliton	<i>OSNR</i>	Optical Signal-to-Noise Ratio
<i>DSO</i>	Digital Storage Oscilloscope	<i>PAM</i>	Pulse Amplitude Modulation
<i>DSP</i>	Digital Signal Processing	<i>PC</i>	Polarization Controller
<i>EA</i>	Electrical Amplifier	<i>PD</i>	Photodiode
<i>EAWG</i>	Electrical Arbitrary Waveform Generator	<i>PM</i>	Power Meter
<i>EDFA</i>	Erbium Doped Amplifier	<i>PON</i>	Passive Optical Fibre
<i>EQ</i>	Equalisation (Adaptive Post-Equalisation)	<i>PRBS</i>	Pseudo-random Bit Sequence
<i>FBT</i>	Feed-Back Taps	<i>PS</i>	Power Splitter
<i>FFT</i>	Feed-Forward Taps	<i>SBS</i>	Stimulated Brillouin Scattering
<i>FSR</i>	Free Spectral Range	<i>SD-FEC</i>	Soft-Decision Forward Error Correction
<i>FWHM</i>	Full Width Half Maximum	<i>SMF</i>	Single Mode Fibre
<i>FWM</i>	Four-Wave Mixing	<i>TNR</i>	Tone-to-Noise Ratio
<i>HD-FEC</i>	Hard-Decision Forward Error Correction	<i>TP</i>	Tapered Fibre
<i>IEEE</i>	Institute of Electrical and Electronics Engineering	<i>VOA</i>	Variable Optical Attenuator
<i>IM/DD</i>	Intensity Modulation Direct Detection	<i>WGM</i>	Whispering Gallery Mode
<i>ITU-T</i>	International Telecommunication Union-Telecommunication Standardization Sector	<i>WDM</i>	Wavelength Division Multiplexing
<i>LPF</i>	Low-Pass Filter	<i>WDM-PON</i>	Wavelength Division Multiplexed Passive Optical Network
<i>MZM</i>	Mach-Zehnder Modulator		

GENERAL DESCRIPTION OF THE THESIS

Topic Introduction

The world has recently experienced dramatic changes in our lives and the services we use due to the pandemic. The telecommunications industry has not been an exception, experiencing a rapid jump in the amount of data transmitted [1], which comes from new services such as high-quality video streaming, video conferencing, augmented and virtual reality, online offices, etc. Today's telecommunications industry generates an increasing amount of carbon dioxide emissions (CO₂) of global emissions, which have increased from 1.4 % in year 2018 [2] to 4 % in year 2021 [3]. This is a serious problem that telecommunications engineers must solve to reduce emissions and support "green thinking".

Therefore, telecommunication infrastructure owners must look for new solutions and technologies for the purpose of improving the network, to be able to cope with similar global crises in the future and to stop the continuous increase in emissions of CO₂ by 1.4 % per year from the telecommunications industry [4]. Metro networks, data centres and passive optical networks generate the largest share of emissions in the entire communications industry. Two fundamental factors to reduce emissions are energy-efficient and low-cost hardware to operate these systems [5].

Modern optical communication networks use wavelength division multiplexing (WDM) technology to transmit large amounts of data, where several individual laser sources (laser arrays) are used to provide WDM channels. The most commonly used are lasers with a distributed feedback array [6]; however, other types of lasers, such as a surface-emitting laser with a vertical resonator [7], are also used in transceivers with a shorter transmission distance of up to 10 km. Such a WDM system, where laser arrays are used as sources of carrier signals, requires high costs, as individual lasers require synchronization. In addition, the wavelengths emitted by laser arrays drift in the range of several GHz due to heating and appropriate guard bands are required to avoid overlapping of adjacent channels as a result of heating. Thus, an efficient solution would be to use one light source for all data channels.

Optical frequency comb (OFC) generators, i.e., multi-wavelength carrier signal sources, offer an energy-efficient and low-cost platform to simplify the optical transceivers widely used in modern communication systems, as well as to reduce energy consumption in optical communication networks. OFC sources generate multiple carrier signals with the same spectral line spacing (from a few GHz to several hundreds of GHz), which meets the recommendation G.694.1 of the Telecommunication Standards Sector of the International Telecommunication Union (ITU-T) [8], to be able to ensure 2ⁿ channels (refer to Fig. 1). This advantage of OFC generators can therefore be used in a WDM transmitter, where an array of individual lasers can be replaced by a single optical frequency comb. So, it significantly simplifies the optical communication network, and changes are only required in the part of the transmitter, where the laser array is replaced, and an additional arrayed waveguide grating demultiplexer (AWG-DEMUX) is inserted. The rest of the network, including receivers, remains unchanged. Existing passive optical network (PON) standards such as next generation passive optical network (NG-

PON2), conforming to ITU-T Recommendation G.989.2 [9] and standards such as Super-PON developed and standardized by the Institute of Electrical and Electronics Engineers (IEEE) P802.4cs working group [10], can be optimised using carrier signals generated in a silicon microsphere and micro-rod Kerr OFC light source.

Aim, Tasks and Theses to be Substantiated

The aim of the Thesis is to develop a whispering gallery mode resonator optical frequency comb light source and integrate it into intensity-modulated optical communication systems.

The following tasks are defined to achieve the aim of the Thesis:

1. To analyse operation principles of whispering gallery mode resonator-based optical frequency comb light sources and possibilities to adjust the resulting optical frequency comb parameters to be used in optical C-band (1530–1565 nm) data transmission.
2. To fabricate silica microspheres and micro-rods in RTU TI SSTIC laboratory for implementation in an optical frequency comb light source.
3. To analyse the performance of 10 Gbit/s NRZ-OOK WDM-PON transmission systems with varying channel numbers (1, 4, 8 channels), spacing between optical carriers (400 GHz, 200 GHz, 100 GHz) and up to 60 km long transmission fibres (SSMF, CSF, NZ-DSF) by integrating numerically and experimentally obtained optical frequency combs in mathematical simulation programs.
4. To evaluate the capabilities of the experimentally developed optical frequency comb light source to ensure 50 Gbaud and 60 Gbaud NRZ-OOK data transmission and 50 Gbaud PAM-4 data transmission over short-reach data centre interconnects.

Thesis statements to be defended

1. It is possible to generate an optical frequency comb in the optical C-band (1530–1565 nm) using fabricated silica resonators.
2. It is possible to generate an optical frequency comb in microspheres and micro-rod resonators with optical carrier power and spacing according to the ITU-T G.694.1 recommendation.
3. Optical frequency comb light source supports up to 10 Gbit/s NRZ-OOK and 8-channel WDM-PON access systems with channel spacing of 100 GHz to 400 GHz, using up to 60 km long SMF lines corresponding to different ITU recommendations, and up to 100 Gbit/s PAM-4 DCI systems.

Scientific Novelty and Main Results

1. A mathematical model of 4-channel 10 Gbit/s NRZ-OOK WDM-PON transmission system based on numerically obtained microsphere-resonator optical frequency comb with 200 GHz spacing.
2. A mathematical model of 8-channel 10 Gbit/s NRZ-OOK WDM-PON transmission system based on numerically obtained whispering gallery mode resonator soliton OFC.

3. A mathematical model of 4-channel 10 Gbit/s NRZ-OOK WDM-PON transmission system based on experimentally developed microsphere-resonator OFC light source providing 393-GHz spaced optical carriers.
4. An experimentally developed whispering gallery mode micro-rod-resonator OFC light source, providing 7 optical carriers with optical power higher than -15 dBm.
5. An experimentally developed 2 km long data centre interconnect system with up to 100 Gbit/s data rate per channel based on a micro-rod-resonator OFC light source.

The results achieved in the course of Thesis development have been applied in the following projects

1. ERDF Industry-Driven Research project “Development of optical frequency comb generator based on a whispering gallery-mode microresonator and its application in telecommunications”, 1.1.1.1/18/A/144, 16.05.2019–15.05.2022.
2. PostDoc project with ERDF funding “Development of optical frequency combs for fiber-optic communication systems”, 1.1.1.2/VIAA/4/20/659, 01.01.2021–30.06.2023.
3. ESF doctoral and academic staff specialization strategic strengthening grant, 8.2.2.0/20/I/008, 01.02.2022–30.09.2023

Structure and Volume of the Thesis

The Thesis has been developed as a thematically related collection of scientific publications dedicated to the research of whispering gallery mode resonator fabrication, optical frequency comb light source development, and its integration in fibre optical communication system using mathematical simulations and performing experiments in the laboratory. The Thesis summarizes the information presented in 6 original scientific journal publications and in one scientific conference (indexed in Scopus, IEEE, Web of Science).

Approbation of Thesis Results and Publications

The main results of the Thesis have been published in 6 original scientific articles, one international scientific conference proceedings (indexed in Scopus, IEEE, Web of Science) and 4 scientific conference proceedings (not indexed in Scopus, IEEE, Web of Science).

Scientific publications in journals

1. **R. Murnieks**, T. Salgals, J. Alnis, A. Ostrovskis, O. Ozolins, I. Brice, A. Sedulis, K. Draguns, I. Lyashuk, R. Berkis, A. Udalcovs, T. Bi, X. Pang, J. Porins, S. Spolitis, P. Del’Haye, V. Bobrovs. Silica micro-rod resonator-based Kerr frequency comb for high-speed short-reach optical interconnects. *Opt. Express*, 2023, vol. 31, iss. 12, pp. 20306–20320. DOI: doi.org/10.1364/OE.488436.
2. **R. Murnieks**, L. Skladova, J. Braunfelds, I. Lyashuk, A. Supe, E. A. Anashkina, A. V. Andrianov, S. Spolitis, V. Bobrovs. Impact of Kerr Optical Frequency Comb Linewidth on the Performance of NRZ-OOK Modulated Fibre Optical Communication

System. Laser Physics, vol. 31, No. 11, art. No. 115101, 2021. ISSN 1054-660X. e-ISSN 1555- 6611.

3. S. Spolitis, **R. Murnieks**, L. Skladova, T. Salgals, A. V. Andrianov, M. P. Marisova, G. Leuchs, E. A. Anashkina, V. Bobrovs. IM/DD WDM-PON Communication System based on Optical Frequency Comb Generated in Silica Whispering Gallery Mode Resonator. IEEE Access, 2021, vol. 9, pp. 66335–66345. e-ISSN 2169-3536. DOI: doi.org/10.1109/ACCESS.2021.3076411.
4. J. Braunfelds, **R. Murnieks**, T. Salgals, I. Brice, T. Sharashidze, I. Lyashuk, A. Ostrovskis, S. Spolitis, J. Alnis, J. Poriņš, V. Bobrovs. Frequency Comb Generation in WGM Microsphere Based Generators for Telecommunication Applications. Quantum Electronics, 2020, vol. 50, No. 11, pp. 1043–1049. ISSN 1063- 7818. e-ISSN 1468-4799. Available from: DOI: doi.org/10.1070/QEL17409.
5. E. A. Anashkina, M. P. Marisova, A. V. Andrianov, R. Akhmedzhanov, **R. Murnieks**, M. D. Tokman, L. Skladova, I. V. Oladyshkin, T. Salgals, I. Lyashuk, A. Sorokin, S. Spolitis, G. Leuchs, V. Bobrovs. Microsphere-Based Optical Frequency Comb Generator for 200 GHz Spaced WDM Data Transmission System. Photonics, 2020, vol. 7, No. 3, pp. 1–16. ISSN 2304-6732. DOI: doi.org/10.3390/photonics7030072.
6. K. Zvirbule, S. Matsenko, M. Parjonovs, **R. Murnieks**, M. Aleksejeva, S. Spolitis. Implementation of Multi-Wavelength Source for DWDM-PON Fibre Optical Transmission Systems. Latvian Journal of Physics and Technical Sciences, 2020, Vol. 57, No. 4, pp. 24–33. ISSN 0868-8257. DOI: doi.org/10.2478/lpts-2020-0019.

The results of the Thesis published in the proceedings of scientific conferences (indexed in Scopus, IEEE, Web of Science)

1. I. Lyashuk, **R. Murnieks**, L. Skladova, S. Spolitis, V. Bobrovs. The Comparison of OFC Generation Techniques for WDM Networks. International Conference Laser Optics (ICLO), Jun. 20–24, 2022. IEEE, pp. 1. DOI: doi.org/10.1109/ICLO54117.2022.9840130

The results of the Thesis presented at scientific conferences (not indexed in Scopus, IEEE, Web of Science)

1. I. Lyashuk, **R. Murnieks**, V. Bobrovs. The evaluation of optical frequency comb generators compared to the conventional transceiver types, 63rd International scientific conference of RTU, Riga, Latvia, October 14, 2022.
2. **R. Murnieks**, I. Lyashuk, T. Salgals, J. Alnis, I. Brice, A. Sedulis, A. Udalcovs, Pang, O. Ozolins, S. Spolitis, V. Bobrovs. Micro-rod resonator-based optical frequency comb for datacentre interconnects, 63rd International scientific conference of RTU, Riga, Latvia, October 14, 2022.
3. **R. Murnieks**. Research on Kerr Optical Frequency Combs for NRZ-OOK Modulated Fibre Optical Communication Systems, First Workshop for ERI on Telecommunication and Networks, March 14–15, 2022.
4. **R. Murnieks**, J. Braunfelds, T. Salgals, S. Spolitis, V. Bobrovs, J. Porins. Evaluation of Optical Frequency Comb Generators Based on a Whispering Gallery Mode

Microresonator and Applications in FOTS, 60th International scientific conference of RTU, Riga, Latvia, October 15, 2019.

Scientific articles published on different topics during the elaboration of the Thesis (indexed in Scopus, IEEE, Web of Science)

1. J. Braunfelds, K. Zvirbule, U. Senkans, **R. Murnieks**, I. Lyashuk, J. Porins, S. Spolitis, V. Bobrovs. Application of FWM-Based OFC for DWDM Optical Communication Systems with Embedded FBG Sensor Network, *Latvian Journal of Physics and Technical Sciences*, No. 2, 2022. ISSN 0868-8257.
2. E. Elsts, A. Supe, S. Spolitis, K. Zakis, S. Olonkins, A. Udalcovs, **R. Murnieks**, U. Senkans, D. Prigunovs, L. Gegere, K. Draguns, I. Lukosevics. Fibre Optical Coupler by Comsol Multiphysics Software, *Latvian Journal of Physics and Technical Sciences*, Vol. 59, No. 5, pp. 3–14, 2022. DOI: doi.org/10.2478/lpts-2022-0036.
3. T. Salgals, J. Alnis, **R. Murnieks**, I. Brice, J. Porins, A. Andrianov, E. A. Anashkina, S. Spolitis, V. Bobrovs. Demonstration of a Fibre Optical Communication System Employing a Silica Microsphere-Based OFC Source, *Opt. Express*, 2021, vol. 29, No. 7, pp. 10903–10913. DOI: doi.org/10.1364/OE.419546.
4. A. Supe, S. Olonkins, A. Udalcovs, L. Gegere, **R. Murnieks**, D. Prigunovs, U. Senkans, J. Grube, E. Elsts, S. Spolitis, O. Ozolins, V. Bobrovs. Cladding-Pumped Erbium/Ytterbium Co-Doped Fibre Amplifier for C-Band Operation in Optical Networks, *Applied Sciences*, 2021, vol. 11, No. 4, art. No. 1702. DOI: doi.org/10.3390/app11041702.
5. A. Supe, S. Spolitis, E. Elsts, **R. Murnieks**, G. Doke, U. Senkans, S. Matsenko, J. Grube, V. Bobrovs. Recent Developments in Cladding-Pumped Doped Fibre Amplifiers for Telecommunications System, 22nd International Conference on Transparent Optical Networks (ICTON 2020), proceedings, Italy, Bari, July 19–23, 2020. DOI: doi.org/10.1109/ICTON51198.2020.9203436.
6. K. Zvirbule, **R. Murnieks**, M. Aleksejeva, J. Braunfelds, I. Lyashuk, V. Bobrovs. Integration of FBG Optical Sensor Network in DWDM-PON Transmission System, *Photonics and Electromagnetics Symposium*, proceedings, China, Xiamen, December 17–20, 2019, pp. 1168–1174. DOI: doi.org/10.1109/PIERS-Fall48861.2019.9021808.

INTRODUCTION

High-quality optical resonators make third-order nonlinear optical effects more efficient by encapsulating radiation in a small whispering gallery mode (WGM) resonator volume. This allows OFC to be obtained using four-wave mixing (FWM) [11]. The generation of OFC has been demonstrated by sending a continuous-wave (CW) pumping laser beam of a certain frequency into a nonlinear WGM resonator [12]. Optical frequency comb, in a broad sense, refers to a spectrum consisting of several carrier signals with the same spectral spacing. Such an optical frequency comb is usually called a Turing comb. There is also a soliton comb when the optical frequency comb is in a phase-matched state [13].

OFC light sources have been used in technologies such as optical clocks, radio frequency photonic oscillators, coherent optical communications, etc. [14]. Several data transmission experiments using optical frequency combs obtained in integrated resonators have already been demonstrated when applying the OFC. For example, when using Si_3N_4 , the total data rate is shown as 170.8 Gbit/s with a return to zero on-off modulation [15], and a WDM data transmission rate of up to 50 Tbit/s over a distance of 75 km was achieved [16]. OFC light sources have also been used in short-range wireless optical communications, shown in [17].

OFC light sources based on spatial WGM resonators [18], such as silica microspheres and micro-rods, are significantly understudied. These WGM resonators are relatively simple to fabricate from standard single-mode fibre (SMF) using optical fibre splicers. In addition, data transmission based on OFC light sources built using these spatial WGM resonators is to be demonstrated. One of the most promising applications is optical fibre transmission systems. OFC light sources based on a WGM resonator are significantly simpler (consisting of one pumping CW laser and a WGM resonator) and smaller (the diameter of the resonator is usually from μm up to mm) than OFC light sources such as mode-matched lasers. WGM resonators make it possible to obtain OFCs centred at a wavelength of 1550 nm with a carrier signal spacing of about tens, and hundreds of GHz, covering more than 500 nm (70 THz) [19] or even several octave bandwidth [20]. It corresponds to optical S, C, L and U communication bands [21]. In terms of stability and power efficiency, the potential WGM resonator-based OFC light source is an ideal candidate for the intensity modulation direct detection (IM/DD) in wavelength-division multiplexing passive optical networks (WDM-PON) to replace the commonly used laser array solution [22].

A general schematic of an OFC light source based on a spatial WGM resonator is shown in Fig. 1. The WGM resonator-based OFC light source consists of the following elements. First, a CW laser source is used as the pumping light source, the radiation of which is sent through a polarization controller (PC) to an erbium-doped fibre amplifier (EDFA) to increase the pumping power to the maximum. The amplified pumping radiation is coupled into the nonlinear resonator using a tapered fibre (TP), an angle-polished fibre, or a prism. An optical bandpass filter (OBPF) is used before the microresonator to filter the EDFA noise. The generated OFC is then out-coupled from the resonator by the same means, sent through an optical splitter and measured by an optical spectrum analyser (OSA). In addition, the OFC is detected by a PIN photodiode (PD) to analyse the frequency comb in the time domain with a

digital storage oscilloscope (DSO). At the output of the OFC light source, the carrier signals are further used in the transmitter (Tx).

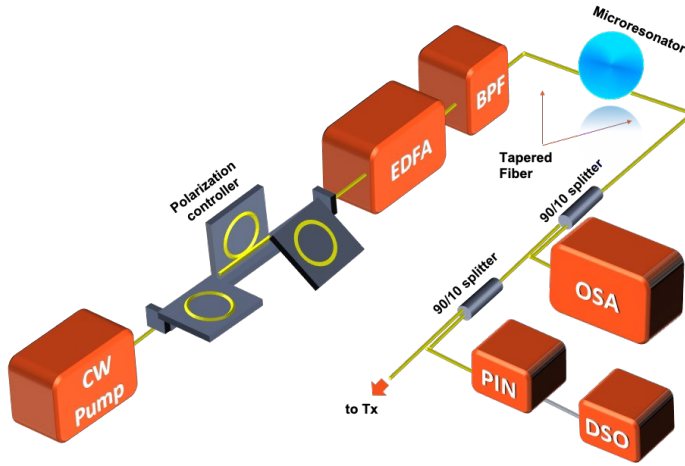


Fig. 1. A typical schematic of a WGM resonator-based OFC light source, where a prism can be used instead of a tapered fibre.

As a result, OFC in microspheres and micro-rods are insufficiently modelled, their parameters are not optimised, as well as their experimental realisation for data transmission in the optical C-band (1530-1565 nm) with the number of channels equivalent to 2^n (e.g., 4, 8, 16 and so on) and data transmissions rates around 10 Gbit/s have not been sufficiently demonstrated.

MAIN RESULTS OF THE THESIS

The development of silica microresonators, i.e., microspheres and micro-rod, was carried out during the doctoral studies, the development of OFC light sources, the acquisition of optical frequency combs, and the evaluation of the use of their carrier signals in both metro-access networks and data centre interconnects were carried out to evaluate the application possibility of OFC obtained in WGM resonators in fibre optic communication systems.

1. FABRICATION OF SILICA RESONATORS AND EVALUATION OF THEIR PARAMETERS AND OPTICAL CARRIER GENERATION FOR DATA TRANSMISSION

Spatial WGM resonators can be mainly divided into two groups – crystalline resonators fabricated by polishing calcium fluoride cylinders (CaF_2) or magnesium fluoride cylinders (MgF_2) and provide a Q -factor of $\sim 10^9$ – 10^{11} [23], and silica resonators, which are developed by melting the end of the fibre by using a heat source, such as CO_2 laser or a gas flame, ensuring a Q -factor of $\sim 10^6$ – 10^{10} .

1.1. Description of Silica Microsphere Fabrication

Typical microspheres with a diameter of several hundred micrometres can be made by melting the tip of a silicon optical fibre using technologies such as electric arc discharge and flame of CO_2 laser [24], [25]. One of the simplest and most reproducible methods is the production of microspheres with a fibre splicer. The Thesis demonstrates the fabrication of microspheres with an optical fibre splicer *Fujikura ARCMaster FSM-100P+*, which allows to repeatedly obtain microspheres with the same parameters as diameter and Q -factor. The manufacturing process begins with constantly bringing the end of a cleaned optical fibre closer to the electrodes while rotating the fibre around its axis so that the microsphere maintains a maximally spherical shape and does not slide down under the influence of its mass. A spherical WGM resonator (microsphere) is thus created under the influence of surface tension forces.

However, to obtain perfectly repeatable microsphere parameters, it is necessary to find optimal splicing parameters. The diameter of the microsphere can be adjusted by adjusting the tuning (or adjustment) of the optical fibre splicer – a parameter that affects the radius of the microsphere, as well as choosing the diameter of the fibre from which the resonator is made. Microspheres of such diameters D as 175 μm and 350 μm are made from standard SMF with a diameter of 125 μm . However, to obtain microspheres with a diameter equal to or greater than 660 μm , coreless fibres with a diameter of 200 μm are required. It was experimentally determined that it takes 42 seconds to obtain 175 μm microspheres but 114 seconds to obtain 350 μm diameter microspheres. As can be seen in Fig. 1.1, as the arc discharge time goes by,

the diameter of the microsphere increases, and the shape becomes more and more close to a sphere.

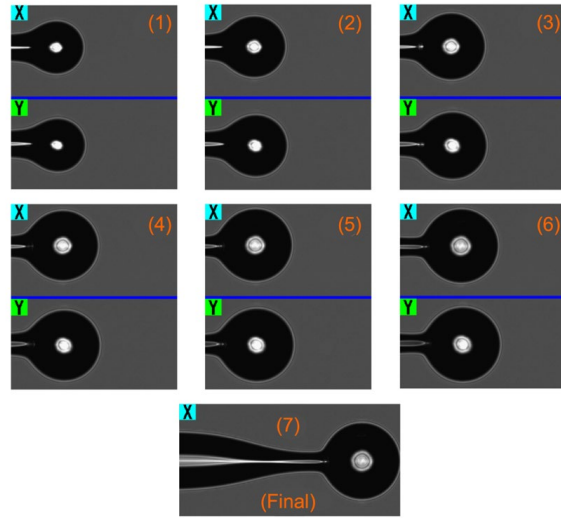


Fig. 1.1. Microsphere shape change and diameter increase depending on arc discharge time.

The choice of diameters is based on the WDM system channel spacing defined in the recommendation ITU-T G.694.1 because it is the diameter that determines the spacing between the lines of the optical frequency comb. Namely, the microsphere diameter d is related to the free spectral range (FSR) through the following relation: $FSR = c/(\pi \cdot d \cdot n_{eff})$, where n_{eff} is the effective refractive index and c is the speed of light in vacuum. Therefore, it is possible to control the FSR by changing the microsphere diameter d . Thus, 175 μm , 350 μm and 660 μm diameters correspond to around 400 GHz, 200 GHz, and 100 GHz FSR , respectively. The optical fibre splicer parameters must be matched to each of the above diameters.

1.2. Description of Silica Micro-rod Fabrication

To make a micro-rod resonator, first, a cylindrical quartz rod must be prepared. The diameter of this cylindrical rod is chosen based on the required spacing between OFC carriers. A micro-rod manufacturing system with CO_2 laser is depicted in Fig. 1.2. A cylindrical quartz rod is attached to an air-cushioned lathe with less than 100 nm of vibrations. This quartz rod is rotated perpendicular to the laser beam. A CO_2 laser beam focused by a zinc selenium (ZnSe) lens is incident on a rotating quartz rod, resulting in the material being cut. In the next step, a resonator is created by focusing the laser beam at different positions along the axis of the quartz rod. During the process of cutting the material, dust is constantly generated; therefore, during the production of the micro-rod, a suction mechanism is needed to collect the dust, which can settle on the microrod and significantly reduce both its stability and the Q -factor. After the primary fabrication process is complete, the cutting area is annealed around with a laser beam, which greatly improves the Q -factor of the microresonator. Using the same fabrication process

and configuration – laser power, irradiation, duration, quartz rod rotation speed, and precise beam positioning – it is possible to recreate identical micro-rods. With this method, it is possible to create several micro-rods with the same parameters on one quartz rod in a relatively short period of time (around 5 min). Figure 1.2 (b) shows five microrod resonators built on a single quartz rod with a diameter of $700\ \mu\text{m}$ D and a $520\ \mu\text{m}$ space between the resonators, but with different curvature radii r (refer to Fig. 1.2 (c)), namely, $250\ \mu\text{m}$, $250\ \mu\text{m}$, $200\ \mu\text{m}$, $175\ \mu\text{m}$, and $150\ \mu\text{m}$ (respectively, from Res1 to Res5). The curvature radius allows adjusting the Q -factor of the resonator because not only the inhomogeneity of the surface of the micro-rod resonator, from which light is reflected and scattered outside the resonator, reduces the Q -factor but also the curvature radius of the micro-rod [26] is important. The curvature helps to retain and focus the light within the resonator mode.

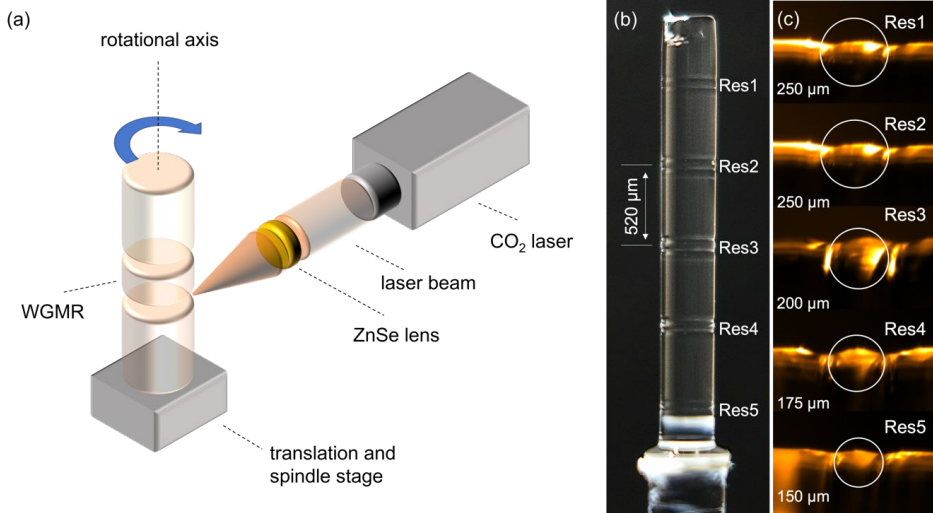


Fig. 1.2. (a) Development of micro-rods on a quartz rod using a CO₂ laser, where a spindle stage is used to rotate the quartz rod and a galvanometer is used to position the laser beam on the ZnSe lens. (b) A picture of 5 fabricated micro-rods on one rod taken under a microscope with a diameter of $700\ \mu\text{m}$ and a space of $520\ \mu\text{m}$ between them. (c) Snapshots of individual micro-rods Res1–Res5, where the white circle indicates different curvature radii r .

Res2 micro-rod WGM resonator (Res2, $D = 700\ \mu\text{m}$ and $r = 250\ \mu\text{m}$) is used in Section 2.3. to obtain a Kerr-OFC with a carrier spacing of $\sim 90\ \text{GHz}$ (89 GHz). This micro-rod WGM resonator is chosen because the combination of resonator diameter $D = 700\ \mu\text{m}$ and curvature radius $r = 250\ \mu\text{m}$ gives the highest measured Q -factor of 2.6×10^7 , compared between the 5 fabricated micro-rod WGM resonators. The measured Q -factor is lower compared to [27], comparable to microspheres ($\sim 10^7$ – 10^9), but higher than the one for integrated resonators ($\sim 10^5$ – 10^6) [28]. The second resonator is also chosen based on experimental observations, as the OFCs obtained in the other micro-rod resonators were significantly affected by stimulated Brillouin scattering (SBS) noise.

1.3. Evaluation of Optical Frequency Comb Generation

The OFC is derived from the nonlinear cascaded four-wave mixing (CFWM) optical effect provided by the Kerr nonlinearity process in optical materials [12]. Therefore, Kerr OFCs can be produced in any resonator made of an optical material with Kerr nonlinearity. OFC generation has been experimentally demonstrated in crystalline [29] as well as fibre ring resonators [30]. Numerically, optical frequency comb in microspheres is simulated based on the Lugiato-Lefever equation using the split-step Fourier method [31].

If the pumping radiation power exceeds the parametric gain threshold power in high Q -factor WGM resonators, the first OFC carriers appear at Stokes and anti-Stokes frequencies with FSR multiples of spacing around the respective pumping frequency. A further increase in pumping power excites the CFWM, which produces higher-order carrier signals, forming the primary OFC. Initially, the carrier spacing Δ is reproduced between the newly created carriers, as CFWM ensures the conservation of energy. In the next step, the secondary carrier signals form sub-combs with a new resonant spacing δ , which is different from the primary spacing Δ . Finally, the sub-combs overlap and form an OFC spectrum, where the spacing between two successive OFC carriers coincides with the FSR of the WGM resonator [19].

The spacing between the OFC carriers is usually equal to the FSR of the WGM resonator [32]. The FSR or wavelength range between two resonances of a WGM resonator can be estimated using Equation (1.1), where a is the major radius of the resonator and n_0 is the refractive index at the frequency of the pumping radiation [33]:

$$FSR_{WGM} = \frac{c}{2\pi a n_0}. \quad (1.1)$$

The spacing of OFC carrier signals in a small range can be adjusted in two ways – by changing the coupling conditions of the pumping radiation or by changing the radiation frequency [34]; in other words, by shifting the pumping frequency relative to the resonance mode frequency of the resonator. Changing the coupling conditions of the pump radiation changes the gap between the resonator and the TP, therefore changing the spacing between the OFC carriers and the Q -factor (increasing the gap increases the Q -factor). The Q -factor is a measure of the sharpness (linewidth of the carrier signal) of a resonance relative to its central frequency, where λ_{res} is the resonance wavelength and full width at half maximum (FWHM) describes the width of the resonance line [35]:

$$Q_{factor} = \frac{\lambda_{res}}{FWHM}. \quad (1.2)$$

In the following, the experiments carried out in this section, the results obtained, and the methods described are promising for telecommunication applications, such as optical transmission systems of multi-wavelength light sources. The structure of OFC light sources is based on a high-quality WGM resonator. Its high Q -factor is at least 2×10^7 , determined by the smooth surface, low internal losses, and radiation coupling in and out from the resonator [35]. In the OFC light source (refer to Fig. 1.3), the radiation is coupled into the WGM resonator through TP. To implement an OFC light source (refer to Fig. 1.3), a SiO₂ microsphere was fabricated, as well as a TP. It should be mentioned that TP is a popular technique for the

radiation input into resonator because it provides high radiation input efficiency, and the TP is relatively easy to fabricate compared to angle-polished fibres or flat waveguides. In addition, the TP can be easily integrated compared to, for example, a prism, which is also often used for radiation input in WGM resonators.

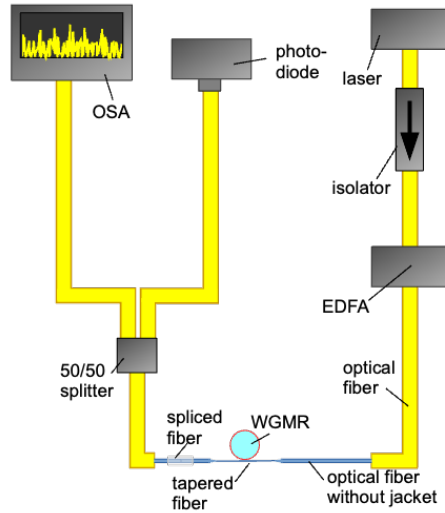


Fig. 1.3. OFC light source based on a SiO_2 microsphere and tapered fibre.

In the OFC light source shown in Fig. 1.3, a 40-mW single-mode optical laser with a central wavelength of 1550 nm is used to generate the optical signal in the transmission part (Thorlabs SFL1550S) in the scanning regime. To generate an OFC, the laser frequency must be tuned to the WGM faster than the resonator warm-up time [36]. The Kerr effect factually creates an OFC instantaneously. Here, the laser current is driven in a triangular shape with a repetition rate of about 1 kHz with a laser frequency deviation of 2 GHz.

The laser output is connected to an optical isolator to protect the laser from reflected signals. The output of the optical isolator is connected to an EDFA to amplify the power of the optical signal. The output power of the EDFA is fixed at 20 dBm. Then, the amplified radiation is fed into the SMF28 single-mode optical fibre (900 μm shielding), which was used to fabricate the TP, and the optical radiation is coupled into the microsphere resonator. The same TP outputs OFC from the microresonator. Then, a Y-type optical power splitter (PS) with a ratio of 50/50 is used in the receiver part to enable parallel OFC measurement. One of the PS ports is connected to a high-resolution OSA (0.01 nm), and the other port is connected to an InGaAs photodetector with a wavelength band of 800–1800 nm. A photodetector detects the OFC signal and sends it to a signal oscilloscope to monitor the resonance mode of the microsphere. To obtain OFC, it is important to control the gap between the TP and the microsphere (explained using the experimental results shown in Fig. 1.5). The air currents that appear around the thin TP and the microsphere displace these two elements. The gap between them changes, changing the power of the radiation injected into the microsphere, causing the OFC spectrum to fluctuate. This necessitates the creation of an isolation box in which to place the TP together with the

resonator to limit air flows and control humidity levels. This type of box also helps protect the elements from dust, which alters the Q -factor of the resonator, as dust particles settle on the surface of the resonator, causing radiation losses.

OFC light source based on TP and SiO₂ microsphere allows to obtain experimentally OFC as shown in Fig. 1.4. As can be seen from the optical spectrum, the OFC carrier spacing is 2 nm or 257 GHz, which is comparable to those studies presented in [21], [31], [34]. In this experiment, the result is obtained by scanning the frequency of the pumping laser and measured by OSA. The absence of some optical carriers can be seen in the OFC spectrum, which can be explained by the laser scanning but also by the mode mixing effect since the microsphere resonator has a wide mode spectrum. When two spatial modes are resonantly aligned at the same wavelength, OFC carrier intensity decreases as power is transferred to another family of modes [37]. So, according to the results, it is possible to obtain an optical frequency comb for optical communication applications; however, optimisation of the parameters and structure of the given OFC light source is required to achieve a time-stable OFC spectrum [36], which is presented in the following chapters of the Thesis.

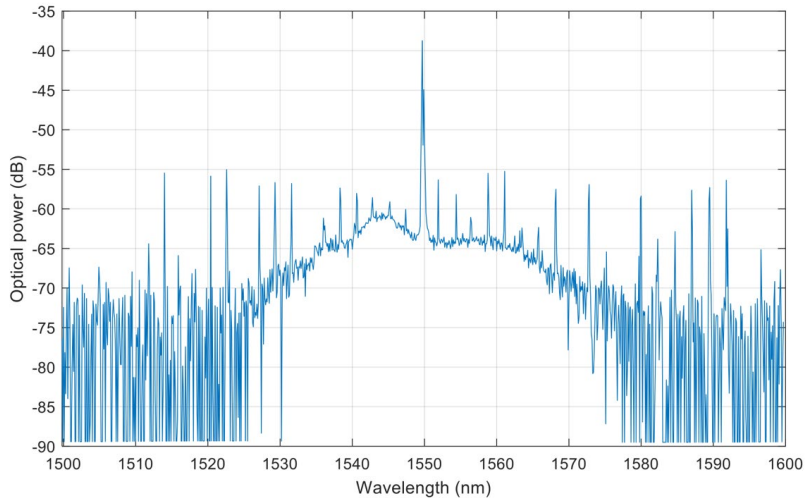


Fig. 1.4. Optical frequency comb obtained in OFC light source (Fig. 1.3).

As mentioned above, changing the light input conditions, i.e., the gap between the TP and the resonator, changes the Q -factor of the resonator. The Q -factor determines how long the pumping radiation circulates in the resonator, and by reducing the coupling losses (increasing the gap), it is possible to increase the Q -factor [14]. A higher Q -factor, in turn, results in a narrower FWHM of the carrier signals. So, it can be said that increasing the gap between the TP and the resonator makes the FWHM of the carrier signal narrower, as shown in Fig. 1.5 (a). The increase in Q -factor is shown in Fig. 1.5 (c). The radiation input conditions in the resonator can be divided into three different regimes [38]. In the first regime, the fibre is located far away (0.57 μm) from the microsphere. The power injected into the resonator is too small (despite the low coupling losses) to overcome the internal losses due to absorption, as seen by the resonance

intensity. For example, in Fig. 1.8 (a), if the gap is $0.47\ \mu\text{m}$, the resonance depth is ~ 0.025 a.u. (refer to Fig. 1.8 (b)), and the Q -factor is $\sim 6 \times 10^6$ (refer to Fig. 1.8 (c)). In the second regime, the radiation power in the resonator is high, but there are significant coupling losses, so the Q -factor is small. For example, if the gap is $0.00\ \mu\text{m}$, then the Q -factor is $\sim 5 \times 10^5$, and the resonance depth is ~ 0.25 a.u. In the optimal regime, there is a balance between the power injected into the resonator and the coupling losses. Considering the mentioned facts, it can be concluded that the optimal gap between TP and microsphere is $0.12\ \mu\text{m}$ or $0.17\ \mu\text{m}$.

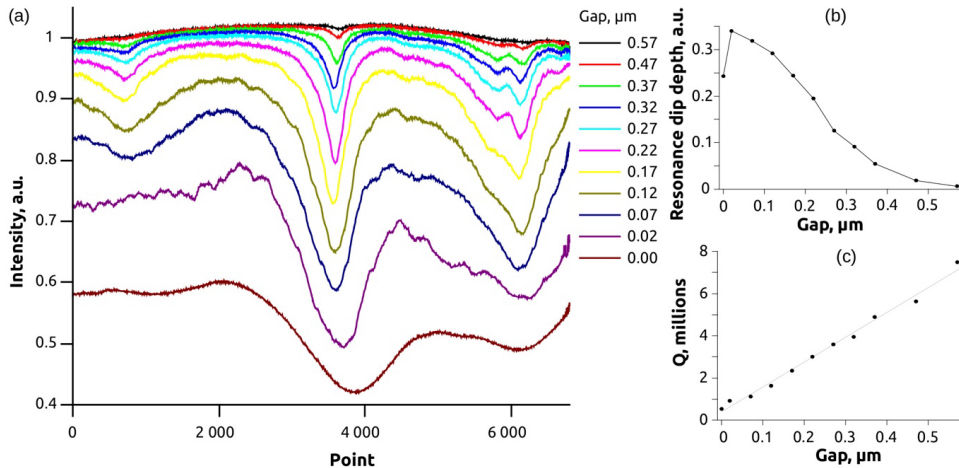


Fig. 1.5. The radiation input conditions depend on the gap between the tapered fibre and the resonator: (a) WGM resonance transmission spectra when the gap is slowly reduced; (b) resonance depth variation; and (c) Q -factor variation.

Summary: From the conducted research and obtained results, it can be concluded that silica microsphere resonators such as microspheres and micro-rods can generate OFC in the optical C band (1530-1565 nm) if an OFC light source is created on their basis. To achieve the generation of a desired OFC, it is necessary to adjust parameters such as pump power and wavelength to match the resonator mode from one of the resonator mode families. To obtain an OFC in the optical C-band (1530–1565 nm), it is necessary to pump the resonator around the 1550 nm wavelength. To adjust the OFC carrier linewidth for a specific application, such as WDM-PON systems, it is necessary to adjust the gap between the TP and the resonator. Namely, by increasing the gap between the TP and the resonator, the bandwidth of the carrier signals becomes narrower (the Q -factor increases, but the power of the carrier signal decreases). The optimal spacing between the TP and the resonator is $0.12\ \mu\text{m}$ or $0.17\ \mu\text{m}$, depending on the combination of Q -factor and carrier power. Finally, the spacing, or FSR, between the OFC carriers can be adjusted by choosing the appropriate resonator diameter – $175\ \mu\text{m}$, $350\ \mu\text{m}$ and $660\ \mu\text{m}$ diameters correspond to, respectively, 400 GHz, 200 GHz and 100 GHz FSR.

Microspheres were created with *Fujikura ARCMaster FSM-100P+* fibre splicer. It was experimentally determined that it takes 42 seconds to obtain $175\ \mu\text{m}$ microspheres but 114 seconds to obtain $350\ \mu\text{m}$ diameter microspheres from a standard SMF with a diameter of

125 μm . Five micro-rod resonators have been fabricated in a relatively short period of time (around 5 min) with CO_2 laser for a single diameter of a silica rod with 700 μm , and different curvature radii of 250 μm , 250 μm , 200 μm , 175 μm , and 150 μm and 520 μm gaps between the resonators. The highest Q -factor, 2.6×10^7 , has been obtained in a second micro-rod resonator comparable to the microspheres ($\sim 10^7$ – 10^9), but higher than for integrated resonators ($\sim 10^5$ – 10^6).

Original publications on the research described in this chapter can be found in **Appendices 1, 4, and 5 of the Thesis.**

2. ANALYSIS OF AN OPTICAL FREQUENCY COMB GENERATION IN MICROSPHERES AND MICRO-RODS CORRESPONDING TO FIBRE OPTICAL TRANSMISSION SYSTEM NEEDS

2.1. Generation of an Optical Frequency Comb in Silica Microsphere with 400-GHz FSR

A simplified schematic of an experimental OFC light source based on a silica microsphere resonator is shown in Fig. 2.1. For the purposes of the experiment, a microsphere with FSR = 400 GHz ($D = 168 \mu\text{m}$) was fabricated using the optical fibre splicer as shown in Fig. 1.1., and, in addition, a 5 cm long TP fibre was made from SMF-28e fibre.

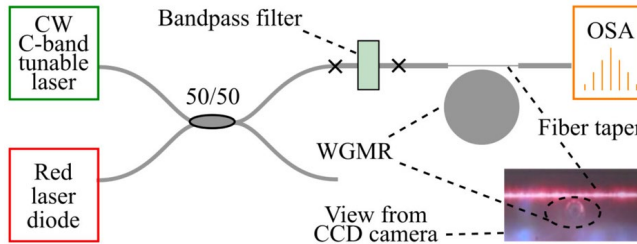


Fig. 2.1. A simplified schematic of the experimental OFC light source.

A WGM resonator is added for a precise three-axis positioning stage (*Thorlabs MAX312D*), which allows for coarse manual positioning as well as fine adjustment of the relative position of the WGM resonator and TP using built-in piezo motors. Coarse positioning of the resonator is performed manually using two CCD cameras, while fine position adjustment is performed by controlling piezo motors with an applied voltage. A view from one CCD camera is shown in Fig. 2.1. A tunable CW radiation laser has been used as the pumping source (*Pure Photonics, PPCL550-180-60*, output power 18 dBm, optical C-band operation, tuning range 60 nm) with a linewidth of 10 kHz. The CW radiation is filtered by a $1550 \pm 10 \text{ nm}$ OBPF to remove the background noise of the CW pumping laser before the radiation enters the resonator through the TP. The output signals from the microsphere are picked up by the OSA (*Yokogawa AQ6370D*, 0.6–1.7 μm). The measured spectral width of the resonant mode of the microsphere is $\delta f = 6.5 \text{ MHz}$. The central frequency of the laser is $f_0 \sim 192.6 \text{ THz}$, hence the calculated $Q = f_0/\delta f = 3 \times 10^7$.

By scanning the frequency (linear modulation) of the pumping laser around 1558 nm, OFC is obtained experimentally. The laser power is set to 16 dBm (before the 50/50 splitter, refer to Fig. 2.1). As a result, an OFC with a carrier signal interval of 393 GHz has been obtained at a small absolute dispersion value by pumping the WGM resonator at a frequency where there is a small anomalous dispersion (refer to Fig. 2.2). FSR 393 GHz roughly corresponds to $n \times$

100 GHz, where $n = 4$, which corresponds to the inter-channel interval values of WDM systems specified in the ITU-T G.694.1 recommendation.

The dispersion of the fabricated silica WGM has been calculated using a method detailed in previous works [39]. Dispersion is determined by a set of discrete points (marked by points in Fig. 2.2 (a) and corresponding to the frequencies of the characteristic modes of the resonator). For easier perception, these points are connected with a line. By comparing the experimentally obtained OFC carrier frequencies with the calculated characteristic frequencies, it can be seen that all the obtained carrier signals can be interpreted as fundamental transverse electric modes (refer to Fig. 2.2 (a), (b), the vertical dashed lines indicate the calculated mode frequencies and the corresponding OFC carrier signals).

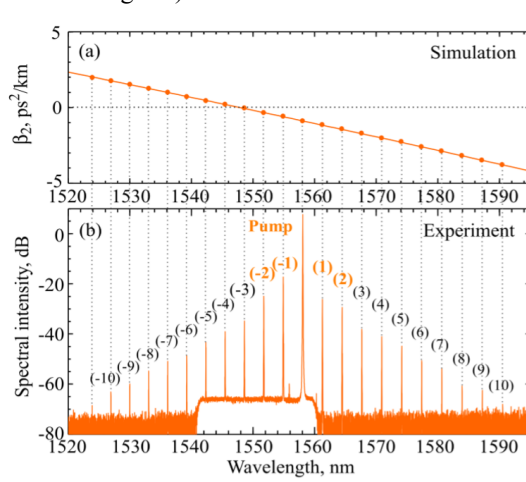


Fig. 2.2. (a) Calculated fundamental transverse electric mode family dispersion of a silica WGM resonator (dots indicate resonator-specific mode frequencies). (b) The spectrum of experimentally obtained OFC. The vertical dotted lines indicate the relationship between the resonator-specific mode frequencies and the OFC carrier signals. The flat plateau from 1540 – 1560 nm is due to the bandpass filter (prior to the TP).

Thus, a stable OFC has been obtained experimentally, providing an OFC light source that contains more than 20 carriers within a single fundamental mode family in and out of the optical C-band. Only four OFC carriers with the highest power, namely (-2), (-1), (1) and (2), are selected for further data transmission analysis. The tone-to-noise ratio (TNR) values of these carriers are about 41 dB, 49 dB, 46 dB, and 43 dB, respectively, while the pumped-radiation carrier has a TNR of about 73 dB.

2.2. Generation of a Dissipative Kerr Soliton Comb in Silica Resonator with 100-GHz FSR

Here, OFCs are numerically simulated by applying the dissipative Kerr soliton (DKS) comb formation mode in a silica resonator. To obtain the desired FSR (in this case 100 GHz) and at

the same time control the parameters so that the dispersion is anomalous in the optical data transmission wavelength range, it is possible to use resonators of different geometries, such as toroids, discs, and spheroids [37]. Figure 2.3 (a) shows a simplified schematic of an OFC light source that uses an axially symmetric silica WGM resonator in which the radiation is injected via a TP. The dynamics of the radiation field circulating inside the resonator can be described by the generalised equation of *Lugiato-Lefever*, which is independent of the geometry of the resonator. A dimensionless form that considers Raman response, anomalous dispersion and cubic dispersion are applied here (standard normalisation, refer to [37]):

$$\frac{\partial E(t, \tau)}{\partial t} = \left(-1 - i\Delta + \frac{i}{2} \frac{\partial^2}{\partial \tau^2} + \frac{b_3}{6} \frac{\partial^3}{\partial \tau^3} \right) \cdot E(t, \tau) + i \left(\int R(s) |E(t, \tau - s)|^2 \right) E(t, \tau) + S, \quad (2.1)$$

where $E(t, \tau)$ is the intra-resonator dimensionless field; τ and t are the normalised fast and slow times, respectively; b_3 is a dimensionless coefficient characterising the cubic dispersion (here $b_3 = 0.01$); Δ is the dimensionless detuning from exact resonance mode closest to the pumping frequency (here $\Delta = 60$); S is the CW pumping radiation field entering the WGM resonator (here $|S|^2 = 65$); $R(t)$ is the Raman response function taken in the common form for silica glass [40]:

$$R(t) = (1 - f_R)\delta(t) + f_R(\tau_1^{-2} + \tau_2^{-2})\tau_1 \exp(-t/\tau_2) \sin(t/\tau_1), \quad (2.2)$$

where $\delta(t)$ is the Dirac delta function; $f_R = 0.18$ is the Raman part in relation to the nonlinear response; $\tau_1 = 12.2$ fs and $\tau_2 = 32$ fs.

The results of the numerical simulation of OFC in DKS mode at a resonator pumping frequency of 193.7 THz (1547.71 nm) are shown in Fig. 2.3. To modulate the DKS optical frequency comb within the framework of Equation (2.1) with consideration of Equation (2.2), a code from *Matlab* is being utilised, the operation of which is based on the split-step Fourier method. The authors in [41] have analysed the effect of the Raman response on DKS (in the absence of cubic dispersion). The research has found such displacement parameters at which an existing fundamental soliton is stable. The effect of Raman nonlinearity is shown to cause an asymmetry of the DKS spectrum with respect to the frequency of the pumping radiation and a shift of the spectrum closer to longer wavelengths, which is also consistent with the results presented in [42]. In this case, the top of the shifted soliton is comparably flat at large values of the shift of Δ . Therefore, the choice of Δ and S parameters is dictated by the results presented in [41]. The FSR of the resonator modes set in the code is 100 GHz (coinciding with a microsphere diameter of about 660 μm) according to the ITU-T inter-channel interval.

The frequency of the pumping radiation is chosen so that the most suitable carrier signals for WDM systems (around 193.1 THz) have the maximum power. The relative spectral intensity of the OFC carrier signals is shown in Fig. 2.3 (b), whereas Fig. 2.3 (c) shows the distribution of the resulting DKS pulse intensity in the time domain with FWHM duration $T_{\text{FWHM}} = 180$ fs. The zoomed-in spectrum near the peak of the soliton is shown in Fig. 2.3 (d). The carrier signal located at the pumping frequency is labelled with (0). It can be seen that the (-6) and (-7) carriers located at frequencies corresponding to 193.1 THz and 193 THz, respectively, have the maximum relative intensity. Eight carrier signals (-3), (-4), to (-9),

(-10) whose power difference does not exceed 0.5 dB can be used for the 8-channel WDM-PON system for further data transmission. For the given study, OFCs with carrier FWHM values of 100 kHz, 1 MHz, 10 MHz and 100 MHz are numerically simulated, where the optical carrier signals in each case are spaced at 100 GHz interval or FSR, which corresponds to the ITU-T G.694.1 recommendation. OFCs with different carrier linewidth values, which are later integrated into the simulation model, are shown in Fig. 2.4.

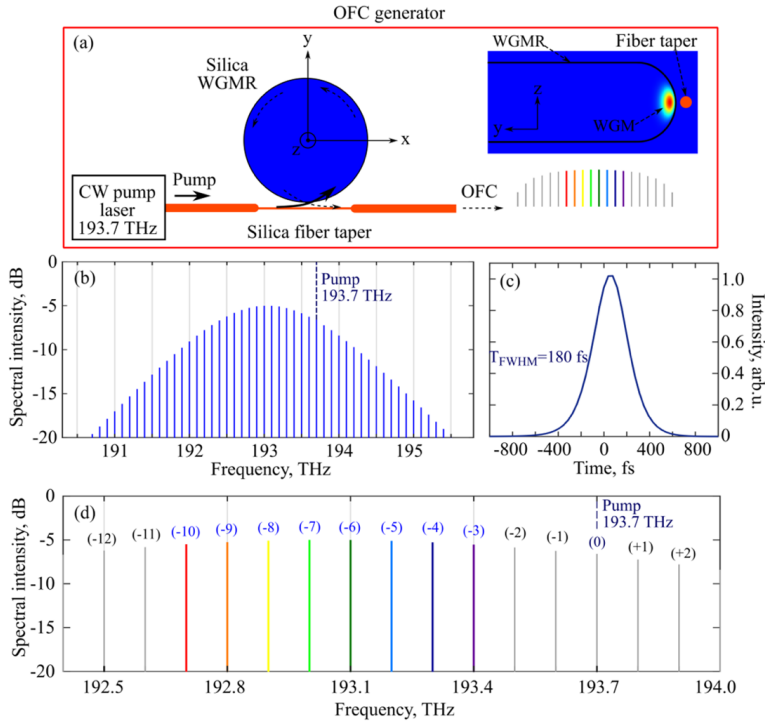


Fig. 2.3. (a) Simplified schematic of an OFC light source. The inset image to the right shows the realisation of a particular edge of the resonator. In simulated OFC DKS regime: (b) optical spectrum; (c) the corresponding power distribution in the time domain; (d) zoomed OFC spectrum at its top.

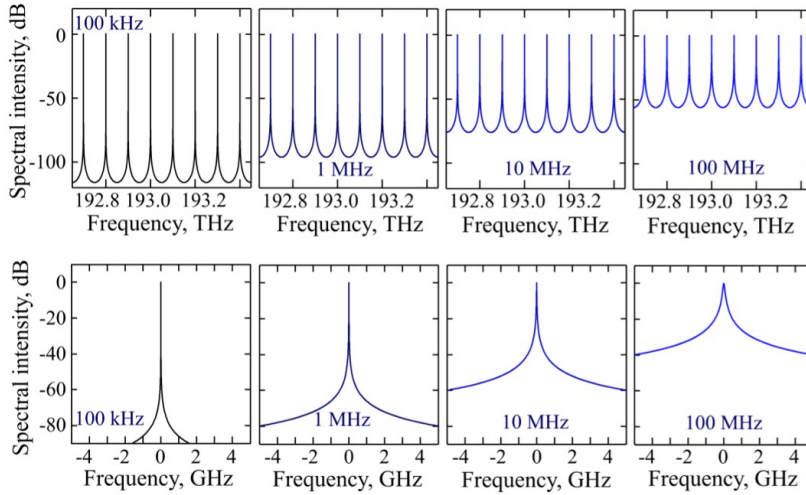


Fig. 2.4. OFC carrier spectra used in simulations of an 8-channel 100 GHz inter-channel spacing WDM-PON system with different carrier signal linewidth values (top row) as well as zoomed centre carrier signals (bottom row).

2.3. Development of an Experimental Optical Frequency Comb Light Source Based on Silica Micro-rod with 90-GHz FSR

The experimental scheme visible in Fig. 2.5 has been used to obtain an OFC in a micro-rod light source. The TP fabricated from a non-zero dispersion shifted fibre (NZ-DSF), similar to previous studies [43], and the silica micro-rod are enclosed in a box to protect them from dust. Inside the box, the humidity is kept below 20 % with the help of a silicon gel desiccant (dryer). In addition, both the pumping source and the box are placed on a vibration-isolating table to minimize the influence of external low-frequency vibrations.

The micro-rod OFC light source consists of a CW laser (*Agilent 81989A*) with a centre frequency of $\lambda = 1555.46$ nm, bandwidth of 100 kHz, optical output power +6 dBm and relative intensity noise -145 dB/Hz. PS, with a 50/50 ratio, splits the pumping laser radiation into two equal parts – in clockwise and counterclockwise directions. These two parts of the radiation are pumped into the micro-rods at the wavelength $\lambda = 1555.46$ nm from both sides. First, the light in each pumping section is sent through a 5 dB fixed optical attenuator (to ensure adequate optical input power of the amplifier) and then sent to the EDFA (in counter-clockwise: *Keopsys PS-CUS -BT-C* and in clockwise direction: *Spectra RED5018*) with fixed output power (up to +23 dBm). Afterwards, the amplified optical signals pass through PCs placed before optical circulators (OCs) to optimise radiation input efficiency. OC is used to eliminate the effect of backscattering light, which can cause instability of the CW laser and lower the amplification efficiency of the EDFA. In clockwise and counterclockwise directions, the light is fed into the TP fibre via optical circulator 1 (OC1) and 2 (OC2). The light signal of the optical frequency comb is sent to the OSA through the return port of OC1 (*Anritsu MS9740A*, 0.03 nm resolution)

to monitor and measure the power of the generated OFC carrier signals. In clockwise and counterclockwise directions, radiation coupled into the micro-rod from both sides ensures the required circulation intensity to achieve OFC generation. When radiation is input in only one direction, some of the optical power is converted to heat, so radiation input in the other direction is required to compensate for optical power losses. Increased stability of the OFC acquisition was obtained by pumping the micro-rod from two sides, splitting the radiation of one laser into two directions. In each direction, the EDFA amplifies the optical power to a fixed level of +23 dBm. A single pumping laser beam in two directions has previously been used in [44]. Finally, the optical circulator OC2 separates the generated OFC. A 10/90 ratio optical splitter captures the output OFC spectrum using OSA-2 (*Advantest Q8384* with 0.01 nm resolution).

The generated OFC is shown in Fig. 2.6 along with a zoomed-in centre frequency comb portion around the pumping wavelength corresponding to the (0) carrier signal. The optical carrier signals generated by the OFC light source are plotted and depicted as (0): $\lambda = 1555.46$ nm, (+1): $\lambda = 1556.18$ nm, (+2): $\lambda = 1556$ nm, (+3): $\lambda = 1557.62$ nm, (+4): $\lambda = 1558.34$ nm, (+5): $\lambda = 1559.06$ nm and (+6): $\lambda = 1559.78$ nm (refer to Fig. 2.6) and these are further selected to demonstrate 50 and 60 Gbaud non-return-to-zero on-off keying modulation (NRZ-OOK) and 50 Gbaud pulse intensity modulation (PAM-4) data transmission over a 2 km long SMF line in Section 3.4. The given carriers are chosen for data transmission experiments because they provide the highest peak power levels above -15 dBm (respectively, 4 dBm, -2.7 dBm, -7.3 dBm, -9.6 dBm, -11.6 dBm, -14.8 dBm and -14.1 dBm), compared to others. The distance between the carrier signals is 89 GHz (~ 0.72 nm). The TNR of these carrier signals is 52.9 dB, 46.5 dB, 41.8 dB, 39.4 dB, 36.8 dB, 34.2 dB and 35.1 dB, respectively.

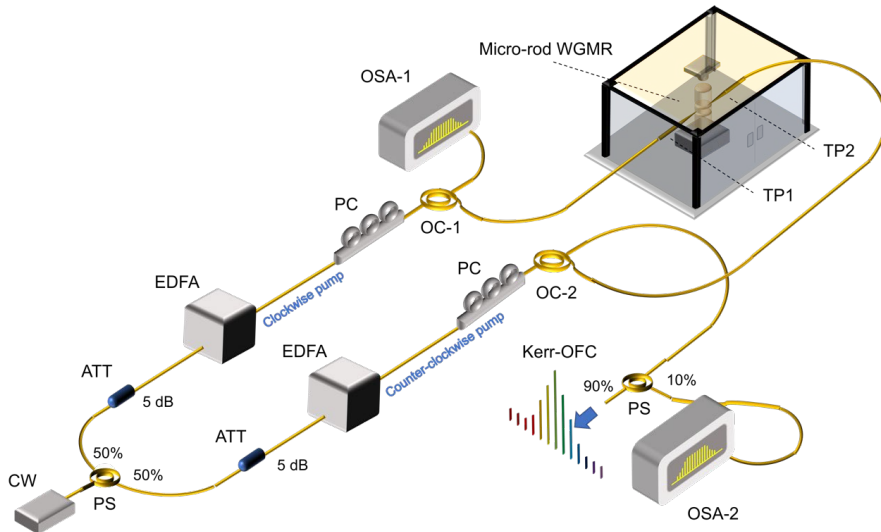


Fig. 2.5. Experimental scheme illustrating a silica micro-rod-based OFC light source for fibre optic transmission systems.

As can be seen in Fig. 2.6 in approximation, optical carrier signals after (+6) have similar performance, however, during the experiment it was observed that these carrier signals are not stable enough to modulate data on them. Additionally, the EDFA, which is used in Fig. 3.15, is

not capable of amplifying the carrier signals after (+6) because they do not provide enough input power, even the (+5) carrier signal is close to the amplified spontaneous emission (ASE) noise level. A solution that would allow the use of carrier signals after (+6) is to first apply an EDFA with a lower input power level.

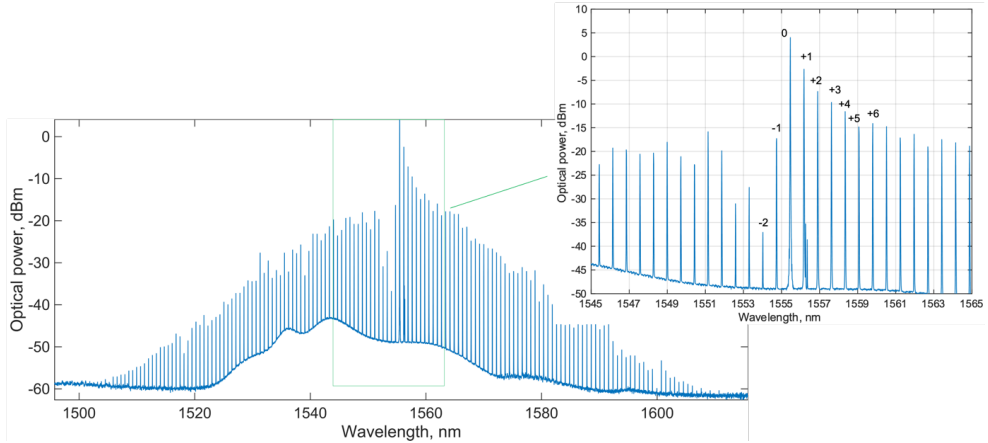


Fig. 2.6. Output spectrum of a silica micro-rod OFC light source with 89 GHz (~ 0.72 nm) comb carrier spacing generated in a Res2 micro-rod resonator with $R = 700 \mu\text{m}$, $r = 250 \mu\text{m}$, and the Q -factor of 2.6×10^7 .

Compared to [45], the obtained OFC is asymmetric – there is a visible drop in the spectrum at shorter wavelengths from the pumped mode. This is explained by mode crossing, that is, at the same wavelength, two modes with opposite polarization exist, and the power is divided between these two modes, and most of the power goes to the opposite polarization mode. The demonstrated OFC is obtained in the Turing state by injecting pumping radiation of 250 mW optical power into the micro-rod through a tapered fibre touching the micro-rod. For most parts of the experiment, the noise performance is close to the noise of the EDFA ASE, except for the optical carrier signal (+1), where the noise comes from the SBS. The OFC is obtained in the second micro-rod (Fig. 1.2) with a pumping power conversion efficiency of about 20 % (250 mW at the resonator input, and the OFC has about 50 mW of optical power over the entire bandwidth). This result is close to [12], where the authors have achieved a similar conversion efficiency but with a lower input power in a $75 \mu\text{m}$ toroidal resonator. In comparison, most soliton OFCs are obtained in integrated resonators with conversion efficiencies of around a few per cent [46].

As can be seen in Fig. 2.6, OFC has a difference of at least 20 dB between the optical power of the individual carrier signals. The reason for large power fluctuations is the Turing state, which is characterized by a decrease in the power of the carrier signals with greater spectral distance from the wavelength of the pumped mode. To ensure similar bit error rate (BER) performance across all carriers in WDM applications, it is important to obtain an OFC with a smooth envelope, as power differences require additional solutions. One possible solution is to obtain the OFC in soliton form, which provides a flatter spectrum. Despite the improved

stability of TNR and soliton carrier signals, obtaining a soliton comb requires stabilizing the circulating optical power of the resonator, which is usually done with an additional laser. However, an additional laser complicates the OFC light source scheme. Another solution to power fluctuations is to amplify each carrier signal to a fixed power level or to use a wavelength-selective switch in the transmission line to equalise the OFC before data modulation.

Optical signal-to-noise ratio (OSNR) is a critical aspect of high-quality WDM data transmission. The minimum ratio should be at least 20 dB [47]. OFC has a long-term stability problem – the power level of OFC carrier signals fluctuates, which causes fluctuations in OSNR and transmitted signal quality. The long-term stability of the OFC carrier signals (refer to Fig. 2.7) obtained from the second ~ 90 GHz (89 GHz) micro-rod (Res-2) has been measured with the TP touching the micro-rod throughout the experiment.

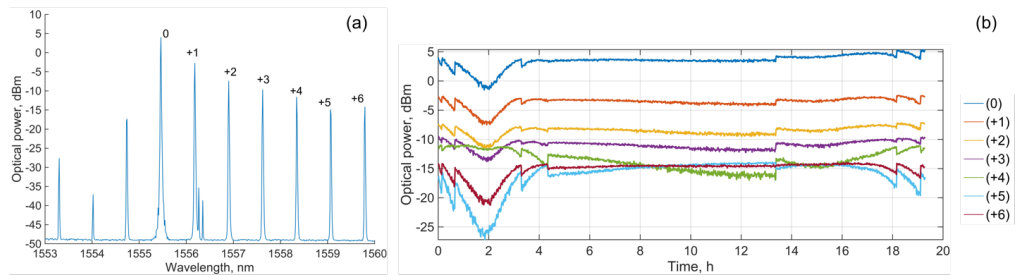


Fig. 2.7. Measured micro-rod OFC light source carrier performance from (0) to (+6):

(a) obtained OFC in the second micro-rod resonator ($D = 700 \mu\text{m}$ and $r = 250 \mu\text{m}$, $FSR \sim 90$ GHz), where the side peaks at the (+1) carrier originate from the SBS. The highest side peak amplitude is 32.3 dB lower than the carrier signal itself; (b) received carrier signal power stability over a 20-hour period.

It has been experimentally observed that the optical carrier signals from (0) to (+6) obtained in the second micro-rod are relatively stable for 20 hours and have different performances due to the simultaneous propagation of several spatial modes in the resonator. In the stability curves from hours 0 to 4, at the 14th hour and the 18th hour, there are fluctuations that need to be explained. The first event is related to the change in temperature, which affects the power of the OFC. Since the temperature is not actively stabilized in the protective box, the temperature inside the protective box is variable in relation to the temperature of the surrounding laboratory environment – during the daytime, around $23.0 \pm 1^\circ\text{C}$. At night, the room temperature drops by 6 degrees, which also explains the first fluctuations from 0 to 4 hours. The sudden spikes at the 14th hour and 18th hour are associated with mechanical displacements between the micro-rod and the tapered fibre. The mechanical displacement causes the mode to circulate inside the micro-rod in a different geometric position, resulting in power spikes.

Despite these power fluctuations, when the external environment is stable or under control, OFC carrier signal power is stable, which can be observed in the time periods of 4 to 14 hours, 14 to 18 hours, and 18 to 20 hours. Thus, it can be said that a stable comb can be obtained in the short term by stabilising the temperature and excluding the influence of the external

environment. It should be mentioned that the power fluctuation trend of the (+4) carrier signal (green curve) is fundamentally different from the others. The reason is the SBS effect, which causes power fluctuations. In the second hour of measurement, the SBS peaks at the (+1) carrier are amplified, taking power from the other carriers. In addition to this, the (+4) carrier signal is also amplified at this moment. The same is true for the green line between 14 and 20 hours. The opposite processes take place between hours 4 and 14, where the SBS peaks and the (+4) carrier signal give power to the other carrier signals, which are therefore amplified. Finally, the measurements were stopped at the 20th hour because the micro-rod heats up, and the SBS effect starts to affect some of the carrier signals. Based on the relatively stable power periods of the carrier signals when the surrounding environment is stable, the OFC carrier signals obtained in the second micro-rod (Fig. 1.3) can be further used in data transmission.

Summary

From the conducted research and obtained results, it can be concluded that OFC with carrier signals can be obtained in the OFC light source based on microsphere and micro-rod resonators according to the requirements of optical communication systems, such as the power and the inter-channel interval defined in the recommendation ITU-T G.694.1. Namely, in the developed microsphere resonator ($D = 168 \mu\text{m}$), pumping it at 1558 nm and an input optical power of about 16 dBm results in an OFC with $FSR = 393 \text{ GHz}$ (approximately corresponds to $n \times 100 \text{ GHz}$, where $n = 4$), where the power of the carrier signals chosen for data transmission is around -20 dBm . In a microsphere resonator ($D = \sim 660 \mu\text{m}$) at a pumping frequency of 193.7 THz, a soliton OFC is numerically obtained with $FSR = 100 \text{ GHz}$, where the power of the carrier signals chosen for data transmission is around -5 dBm and power fluctuations up to 0.5 dB (before data modulation the power is smoothed to 0 dBm). Bidirectionally pumping the micro-rod resonator at 1555.46 nm results in an OFC with $FSR = 90 \text{ GHz}$, where the power of the carrier signals selected for data transmission is above -15 dBm with relative stability over a 20-hour period in a stable environment.

Original publications on the research described in this chapter can be found in **Appendices 1, 3, and 4 of the Thesis.**

3. EVALUATION OF MICROSPHERE AND MICRO-ROD OPTICAL FREQUENCY COMB LIGHT SOURCE IMPLEMENTATION IN HIGH-SPEED DATA TRANSMISSION SYSTEMS

3.1. Development of the IM/DD 4-channel 200 GHz Spaced WDM-PON System Based on Microsphere OFC Light Source

A simulation model of a WDM-PON transmission system with 4 channels and an inter-channel spacing of 200 GHz is shown in Fig. 3.1.

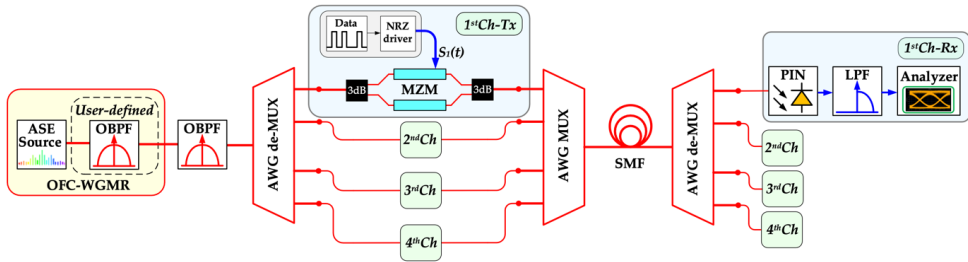


Fig. 3.1. Simulation model of an IM/DD WDM-PON system with 4 channels and an inter-channel spacing of 200 GHz based on a silica microsphere-based OFC light source.

ASE optical light source output with high output power up to 23 dBm and spectral power density -6 dBm/nm in the range 1528–1630 nm is connected to a user-defined OBPF, in which the OFC spectrum obtained previously on a silica microsphere is uploaded. The OFC is then filtered by a second OBPF of 3-dB bandwidth of 750 GHz to extract four optical carrier signals for further application in transmitters. The 4 OFC light source carrier signals are decoupled from each other using AWG-DEMUX corresponding to WDM-PON architecture. Each AWG-DEMUX channel has a 3-dB bandwidth of 87.3 GHz and an inter-channel spacing of 200 GHz. The optical signal spectrum at the output of a user-defined OBPF, the resulting 4-carrier optical carrier signal after the second OBPF, and the modulated optical carrier signals at 10 Gbit/s data channel at back-to-back (B2B) transmission are respectively shown in Figs. 3.2 (a), (b) and (c).

The separated OFC carrier signals are fed into a Mach-Zehnder modulator (MZM). The electrical data signals $S(t)$ modulated by the MZM are provided by a pseudo-random bit sequence (PRBS) generator using a non-return-to-zero (NRZ) driver that generates electrical NRZ signals at a bit transmission rate of 10 Gbit/s. Each MZM has a 3-dB bandwidth of 12 GHz and a maximum and minimum level difference of 20 dB [48]. The optical signals from each transmitter (Tx) are combined using an arrayed waveguide grating multiplexer (AWG-MUX) and transmitted over a 20 to 60 km ITU-T G.652 SMF line with 0.02 dB/km attenuation and 16 ps/nm/km dispersion coefficient at 1550 nm wavelength. The given transmission distance is chosen according to the NG-PON2 standard (ITU-T G.989.2). After transmission, the optical signals are separated by AWG-DEMUX and sent to the specific receivers (Rx). Rx consists of

a PIN photodetector with a 3-dB bandwidth of 12 GHz, a sensitivity of -18 dBm at BER 10^{-12} and a responsivity of 0.65 A/W. The received electrical signal is then filtered by a low-pass filter (LPF) having a 7.5 GHz 3-dB electrical bandwidth. The obtained BER results of electrical signals with respect to SMF line length up to 60 km for NRZ-OOK modulated 4-channel IM/DD WDM-PON transmission system with 200 GHz inter-channel spacing are shown in Fig. 3.3.

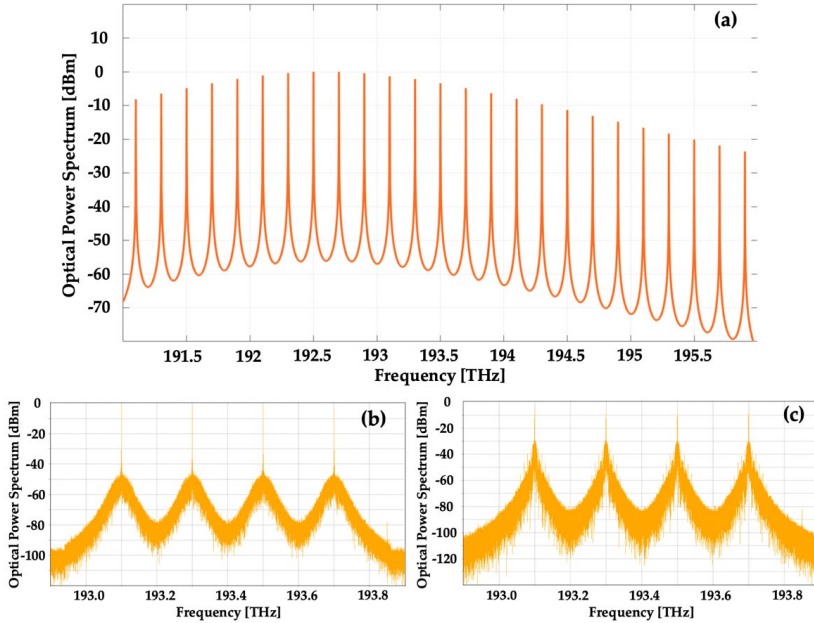


Fig. 3.2. Optical spectra: (a) after a user-defined OBPF with an integrated OFC light source; (b) four optical carriers extracted from an OFC light source after a second OBPF; (c) modulated optical carriers after B2B transmission.

Regarding BER performance, channel 1 (193.1 THz) is the worst-performing. The highest system performance in terms of BER is achieved with channel 4 (193.7 THz), where the BER of the received signal after 60 km SMF line transmission is 4.5×10^{-30} . After 60 km of transmission, the received BER of the worst-case 1-channel is 9.1×10^{-4} . Thus, it can be concluded that OFC light source carrier signals with 200 GHz spacing can provide 10 Gbit/s NRZ-OOK modulated signal transmission for optical link distances of 40 km and 60 km in the IM/DD WDM-PON transmission system.

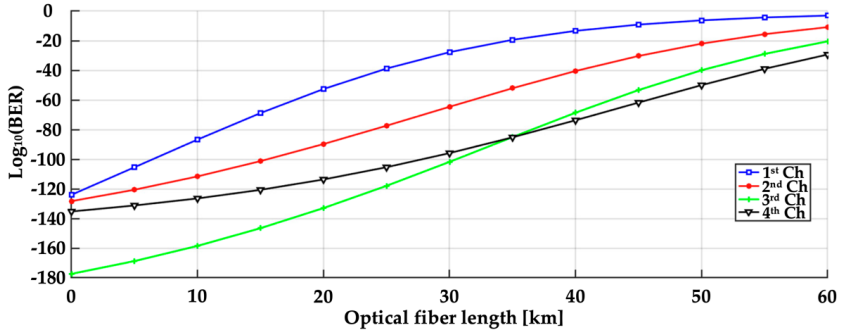


Fig. 3.3. 10 Gbit/s NRZ-OOK modulated 4-channel 200 GHz WDM-PON system BER changes of each channel depending on the length of the transmission line, using the carrier signals of the microsphere-based OFC light source.

3.2. Development of the IM/DD 4-Channel 400 GHz Spaced WDM-PON System Based on a Microsphere OFC Light Source with Different Optical Fibre Transmission Lines

To analyse the performance of the WDM-PON transmission system based on the OFC light source, a simulation model has been developed in the *VPIphotonics* simulation environment. A typical IM/DD WDM-PON system model with 4 channels and 393 GHz channel spacing is shown in Fig. 3.4. The first part is the OFC light source, whose optical parameters are based on the experimental OFC light source. The carrier signals obtained in the OFC light source are used for each data transmission channel. In the simulation model, the experimental comb is integrated through an OBPf with a 3-dB bandwidth of 1720 GHz, which filters the spectral range with four selected OFC carriers of comparable optical power, which are marked in Fig. 2.2 with digits of -2, -1, 1, and 2. The respective frequencies are 193.207 THz, 192.814 THz, 192.028 THz, and 191.635 THz.

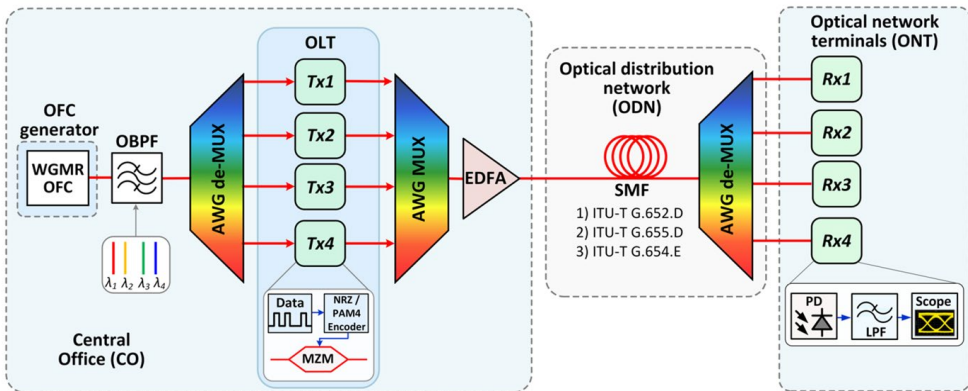


Fig. 3.4. Simulation model of the OFC light source performance and received signal quality evaluation of WDM-PON transmission system with 4 channels and inter-channel spacing of 393 GHz.

The second part of the circuit is the optical line terminal (OLT), where the transmitter (Tx) array is located. First, an AWG-DEMUX with a channel spacing of 400 GHz and a single channel of 3-dB bandwidth of 75 GHz separates each of the four carrier. Each of the carrier signals is sent to its own specific transmitter, where an MZM modulator with a 3-dB bandwidth of 12 GHz and a maximum and minimum power difference of 20 dB imposes 10 Gbit/s data signals on each carrier signal. The transmission speed of 10 Gbit/s corresponds to the 10-gigabit symmetric passive optical network standard and allows the use of a 10 GHz transceiver. The logical data signal with a transmission rate of 10 Gbit/s is obtained from the PRBS generator and converted into the NRZ electrical line signal. Both actions are represented by the "Data" block in Fig. 3.4. After modulation by MZM, the optical signals are combined with AWG-MUX, which has the same parameters as AWG-DEMUX. The combined signal is passed through an EDFA amplifier with a gain of 20 dB to compensate for the attenuation of the multiplexer and demultiplexer units and the MZM modulator and to compensate for the attenuation that will occur during transmission, thus increasing the system's overall power budget.

The third part of the circuit is the optical distribution network (ODN), over which the pre-amplified data channel signals are transmitted. During the simulation, the transmission fibres (the most widely used in the industry, standard SMF [49], NZ-DSF [50] and cut-off wavelength fibre (CSF) [51]) are successively changed to investigate the carrier signal performance of the OFC light source under different transmission conditions. The transmission line length is changed from 0 km (case of B2B) to 70 km, which meets and exceeds the conditions defined for NG-PON2 within the recommendation ITU-T G.989.2 [9]. The selected optical fibres are Corning's most widely produced and used in the optical communications industry. The first fibre is a standard SMF compliant with recommendation ITU-T G.652.D, the second fibre NZ-DSF compliant with the recommendation ITU-T G.655.D, the third type of optical fibre is CSF compliant with the recommendation ITU-T G.654.E. After transmission, each data channel is demultiplexed with the same AWG-DEMUX filter as in the central office (CO) and sent to the specific receiver (Rx) in the optical line terminal.

The fourth part of the circuit is the optical line terminal (ONT), where the receivers are located. Each receiver consists of a PIN photodetector with a 3-dB bandwidth of 12 GHz and a sensitivity of -18 dBm, which corresponds to $BER = 10^{-12}$ and a reflectivity of 0.65 A/W. After the PIN, a 4-pole LPF with a 3-dB bandwidth of 7.5 GHz is used to filter out the noise generated during signal transmission and processing. Then, the electrical signal analyser is used to measure the signal shape and evaluate the signal quality by BER.

To evaluate system performance, Figs. 3.5 and 3.6 show BER characteristics depending on the length of the optical transmission line and the received signal power level. The BER values are taken for the worst data channel that in Fig. 2.2 is marked as the carrier (2) or it is channel 4, which has the lowest power level compared to the other channels. A hard-decision forward error correction (HD-FEC) threshold of 1×10^{-3} is used for WDM-PON system evaluation [52]. Using the selected transmission fibre types – SMF, NZ-DSF and CSF, the BER value decreases with increasing distance, as shown in Fig. 3.5.

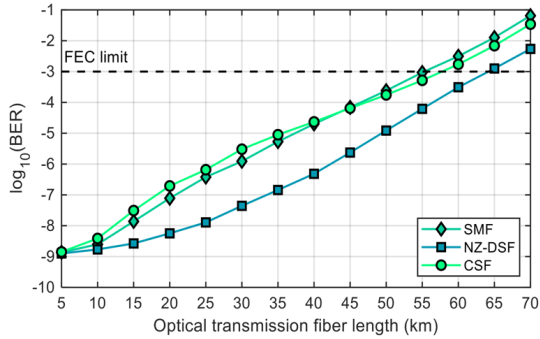


Fig. 3.5. Characteristic curve of BER value change for 10 Gbit/s NRZ-OOK WDM-PON transmission system with applied OFC light source, depending on the length of SMF, NZ-DSF and CSF transmission fibres.

The maximum achievable transmission distance where the BER value is below the HD-FEC threshold is 64 km, 57.5 km and 55 km when using NZ-DSF, CSF and SMF transmission fibre, respectively. As can be seen in Fig. 3.5, with all the selected fibre types, a transmission distance of 20 km can be achieved, which is a typical reach of PON networks, as well as a distance of 40 km. Evaluating the signal quality, it can be concluded that data transmission is possible at 40 km SMF, NZ-DSF and CSF transmission distance, and the values of the received BER signal prior to the FEC are 2×10^{-5} , 4.8×10^{-7} and 1×10^{-5} if SMF, NZ-DSF and CSF transmission fibres are used in the ODN network part respectively. On the other hand, NG-PON2's maximum distance of 60 km can be reached if only NZ-DSF optical fibre is used. These results can be explained mainly by the difference in the chromatic dispersion (CD) coefficients and slight differences in the attenuation coefficient. It is necessary to use CD compensation to achieve longer transmission distances, that is, to reduce the BER value.

For an objective performance evaluation, Figs. 3.6 (a) and 3.6 (b) show the variation of the BER value depending on the received power level at 20 km and 40 km transmission, respectively. BER characteristics are not shown at 60 km because the BER values achieved by SMF and CSF are below the HD-FEC threshold. As can be seen in Figs. 3.6 (a) and (b), the CSF optical fibre shows the worst performance in comparison, as it has the highest CD factor (23 ps/nm/km) and thus the largest dispersion-induced power penalty. The best system performance is achieved with NZ-DSF fibre because it has the lowest CD factor (4 ps/nm/km), and it should be noted that the attenuation differences have a negligible effect on the overall performance difference.

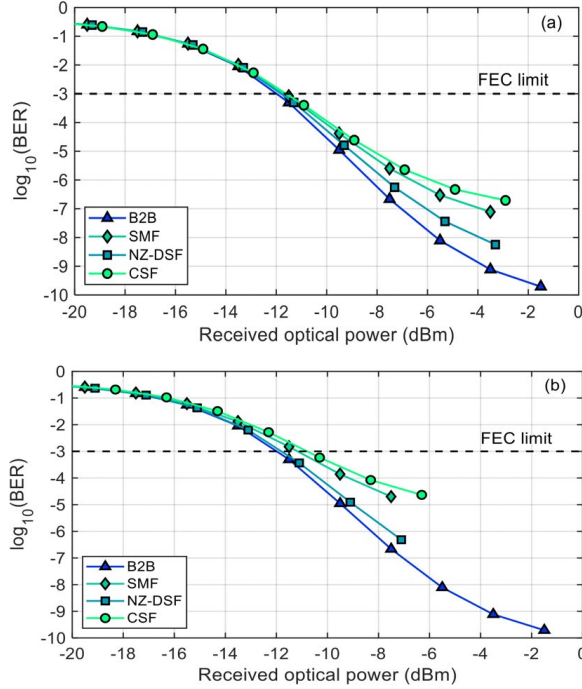


Fig. 3.6. Characteristic curve of BER value variation for 10 Gbit/s NRZ-OOK WDM-PON transmission system as a function of received power level for B2B transmission and at (a) 20 km and (b) 40 km transmission distances.

By evaluating the obtained results (such as the BER characteristic curves as a function of the transmission distance for all three selected types of transmission fibres) in a simulation, it can be concluded that the demonstrated silica microsphere-based OFC light source providing optical carriers with a spacing of 393 GHz is capable of providing BER values below the HD-FEC threshold at a transmission distance of 40 km in 10 Gbit/s NRZ-OOK modulated 4-channel IM/DD WDM-PON system, using both SMF, NZ-DSF and CSF optical transmission fibre.

3.3. Development of the IM/DD 8-Channel 100 GHz Spaced WDM-PON System Based on a Microsphere OFC Light Source with Different Optical Carrier Linewidth Values

Different applications of optical communication networks have different requirements for the FWHM of the OFC carrier signal. A narrow linewidth is important for coherent transmission [53]; for example, an OFC with a linewidth of 14.8 Hz has been used for transmission with a multi-level quadrature pulse amplitude modulation format. On the other hand, in IM/DD communication systems, it is possible to achieve BER values below the HD-FEC threshold 1×10^{-3} using a larger carrier FWHM, and linewidth differences between

carriers of the same OFC may be neglected. Therefore, the performance of NRZ-OOK 8-channel WDM-PON system with 100 GHz inter-channel spacing is demonstrated below (conforms to recommendation of ITU-T G.694.1) depending on the different bandwidths of the OFC carrier signals – 100 kHz, 1 MHz, 10 MHz, and 100 MHz. The different OFC carrier linewidths – 100 kHz, 1 MHz, 10 MHz, and 100 MHz – result in different optical pulse spreading due to the CD of the transmission fibre. To generalise the following study, the OFC light source is presented as a black box, where both a microsphere and a micro-rod can be used as a resonator, as well as OFC light sources of other architectures. The central frequencies of the applied OFC carriers (192.7–193.4 THz) and their spacing of 100 GHz coincide with the centre frequencies of the Super-PON standard channels – FSR set 1 in the optical C-band (192–193.5 THz). In addition, the WDM-PON transmission distance of 50 km matches the network reach defined by Super-PON [10].

To evaluate the capabilities of the obtained OFCs with different bandwidths (refer to Section 2.2 and Fig. 2.4) to provide data transmission in an optical communication system, the *VPI Photonics Design Suite* “Transmission Maker” model of the NRZ-OOK 8-channel WDM-PON system (refer to Fig. 3.7) with an integrated OFC light source has been created. From the output spectrum of the OFC light source, 8 carrier signals are separated by an AWG-DEMUX with a 3-dB bandwidth at 75 GHz, each of which is sent to its own transmitter. PRBS with a bit sequence length of $2^{15}-1$ and the transmission rate of 10 Gbit/s is encoded in NRZ format and modulated in the amplitude of the carrier signal with MZM (bandwidth 12 GHz, maximum and minimum power difference of 20 dB). After modulation, the data channels are combined with an AWG-MUX with a 3-dB bandwidth of 75 GHz and amplified by an EDFA by 5 dB. It is important to note that the use of an EDFA will result in a higher BER value only due to a lower OSNR (the amplifier reduces the OSNR by 4 dB) and not due to the spectral broadening of the signal.

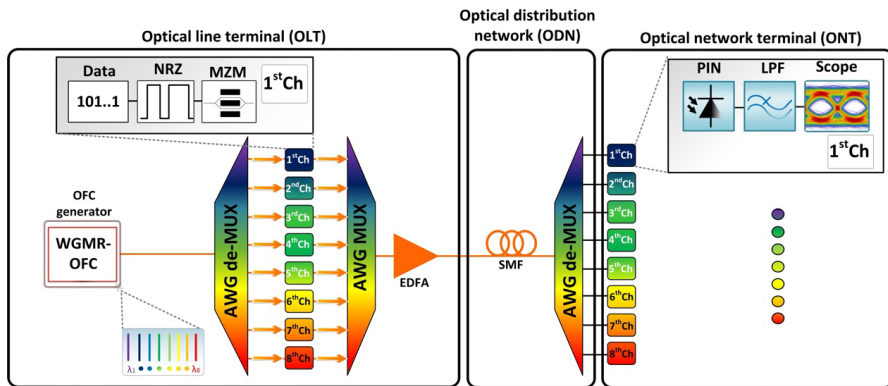


Fig. 3.7. Simulation model of NRZ-OOK modulated WDM-PON data transmission system with 8 channels and 100 GHz spacing based on OFC light source.

After combining the optical signal, it is transmitted through ODN over standard SMF fibre ($\alpha = 0.2$ dB/km, $D = 17$ ps/nm/km at 1550 nm). During the study, the transmission fibre length is varied from 20 to 50 km, where the maximum distance corresponds to Super-PON. When

transmitting an optical signal, each channel is routed to the receivers by means of an AWG-DEMUX (3 dB bandwidth at 75 GHz). Each receiver consists of a PIN photodetector (3 dB bandwidth 12 GHz, sensitivity -18 dBm with $BER = 10^{-10}$, optical power conversion factor 0.65 A/W), LPF with 3-dB bandwidth 8 GHz, which filters out the noise, and from the DSO which captures the eyelet pattern, analytically measures the BER value with the help of the Q -factor and the complementary error function “erfc”.

To evaluate the performance of an 8-channel, 50-km long WDM-PON with 100 GHz spacing using an OFC light source carriers with different linewidths, first, the BER correlation plots are used where the results are shown with a smooth OFC envelope, as seen in Fig. 3.8. The power of the OFC carriers can be smoothed with a spectral filter. In addition, the correlation plots of TNR and BER versus OFC linewidth at 20, 40 (corresponding to NG-PON2) and 50 km (corresponding to Super-PON) transmission distances are shown. Finally, eye diagrams are provided at 50 km data transmission for OFC linewidths 100 kHz, 1 MHz, 10 MHz and 100 MHz. All results are presented for the worst-performing channel in terms of BER value, which in this case is channel 2 with a centre frequency of 192.8 THz, shown in Fig. 2.3 as channel (-9) . The BER values of the received signal (Fig. 3.8) are taken as a function of the average received power at the specified OFC carrier linewidths. Correlation plots are taken using a tunable optical attenuator (VOA) before the PIN photodetector.

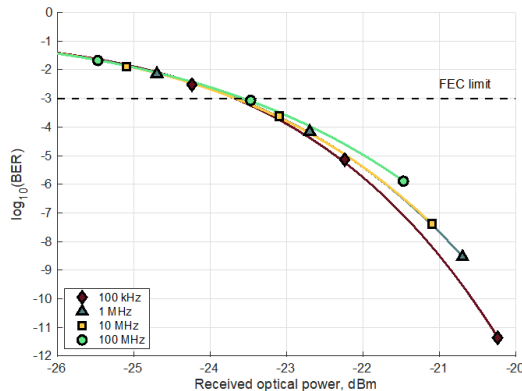


Fig. 3.8. Variation of BER value of NRZ-OOK modulated 10 Gbit/s signal regarding received optical power for linewidths 100 kHz, 1 MHz, 10 MHz and 100 MHz at a transmission distance of 50 km based on OFC with optical power equalised optical carriers.

Since dispersion effects affect the 100 MHz signal the most, this results in lower received power and, therefore, lower BER values. The BER values at a transmission distance of 50 km and a flat OFC envelope vary from 1.3×10^{-6} up to 4.8×10^{-1} for a 100 MHz optical carrier. In comparison, the best performance is shown by the 100 kHz optical carrier, where the BER values at a transmission distance of 50 km vary from 4.4×10^{-12} up to 4.7×10^{-1} . As seen in Fig. 3.8, receiver sensitivity (defined at the HD-FEC threshold of 1×10^{-3}) for the worst-performing channel is -23.9 dBm, -23.8 dBm, -23.7 dBm, and -23.6 dBm for 100 kHz, 1 MHz, 10 MHz, and 100 MHz linewidth values, respectively. The power penalty to reach the defined HD-FEC threshold (1×10^{-3}), if compared to 100 kHz, is 0.1 dB, 0.2 dB, and 0.3 dB

appropriately for 1 MHz, 10 MHz, and 100 MHz. Such power penalty differences can be neglected.

For an optical frequency comb, one of the most important parameters is the TNR of the carrier signals, which is reduced during data transmission, but to ensure *BER* values lower than the HD-FEC threshold, the TNR value before the PIN must be sufficient (for a 10 Gbit/s NRZ-OOK signal, such value corresponds to 10 dB [54]). Therefore, the TNR performance at the studied non-carrier line widths has been shown in Fig. 3.9, which allows us to evaluate the influence of the TNR value of OFC lines on data transmission since the TNR value decreases at a larger line width. Namely, at 100 kHz, 1 MHz, 10 MHz, and 100 MHz, the respective TNR values of the optical carrier signals are 116.1 dB, 96.1 dB, 76.1 dB, and 56.1 dB. As shown in Fig. 3.11, with a linewidth (bandwidth) of 100 kHz, the TNR values are the highest – 53.6 dB, 53.5 dB and 54.3 dB, and at 100 MHz, they are the lowest – 52.3 dB, 52 dB and 51.9 dB, shown at 20 km, 40 km, and 50 km transmission distances respectively.

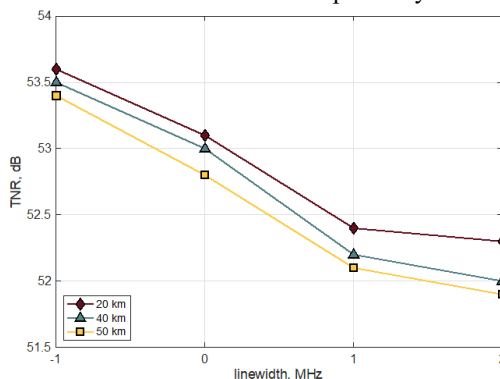


Fig. 3.9. Changes in the TNR value before the PIN photodetector depending on the linewidth values of the optical carrier at 20 km, 40 km, and 50 km transmission distances.

The TNR values directly affect the *BER* values of the received signal; consequently, in Fig. 3.10, *BER* values of the signal as a function of linewidth at 20 km, 40 km and 50 km transmission distance are shown. As can be seen in Fig. 3.10, the *BER* values coincide with the decrease of the TNR value in Fig. 3.9. The lowest *BER* values are provided by a 100 kHz linewidth, where *BER* at a 20 km transmission distance is 3.5×10^{-129} , which corresponds to error-free transmission, and 4.8×10^{-26} and 4.4×10^{-12} at a transmission distance of 40 km and 50 km, respectively. The highest *BER* values are achieved at 100 MHz linewidth, where the *BER* is 3.4×10^{-26} , 2.3×10^{-11} and 1.3×10^{-6} at a transmission distance of 20 km, 40 km, and 50 km, respectively.

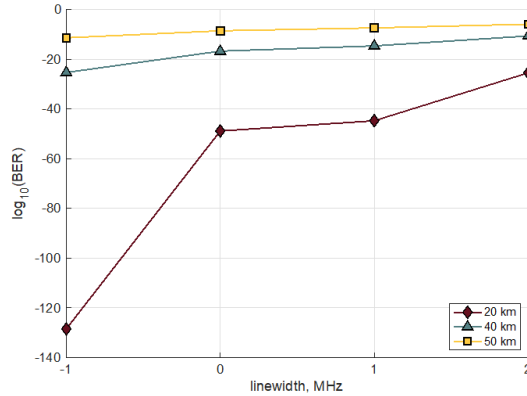


Fig. 3.10. Changes in *BER* values depending on the linewidth of optical carrier signals at 20 km, 40 km, and 50 km transmission distance.

Figure 3.11 shows the received signal quality of channel 2 after 50 km long ODN transmission for all investigated values of carrier linewidth. As shown in Fig. 3.11, the *BER* values are below the specified HD-FEC threshold, where the range of *BER* values between all channels of the received signal are $4.4 \times 10^{-12} - 2.7 \times 10^{-12}$, $2.9 \times 10^{-9} - 4.3 \times 10^{-11}$, $4.1 \times 10^{-8} - 3.2 \times 10^{-11}$ and $1.3 \times 10^{-6} - 1.2 \times 10^{-6}$ (the first value corresponds to the channel with the lowest *BER* performance, and the second value corresponds to the channel with the highest *BER* performance).

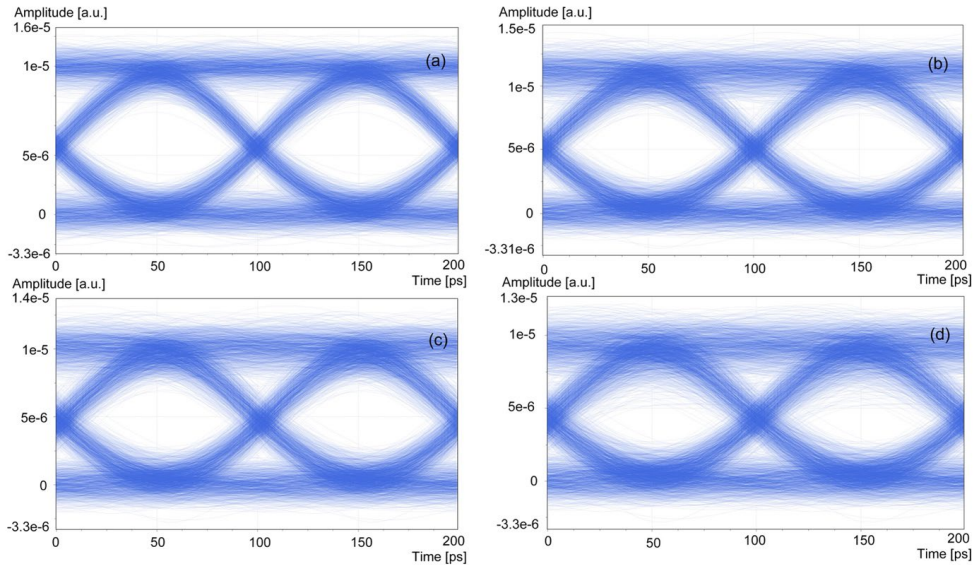


Fig. 3.11. Eye diagrams of the received signal after 50 km transmission over an 8-channel, 100 GHz spacing WDM-PON system operating at a data rate of 10 Gbit/s, using standard SMF for channel 2 studied with carrier linewidth values of (a) 100 kHz, (b) 1 MHz, (c) 10 MHz, and (d) 100 MHz.

The *BER* values obtained after 50 km of standard SMF fibre transmission length are well below the HD-FEC threshold. Therefore, it is possible to use OFC with linewidth values of 100 kHz, 1 MHz, 10 MHz, and 100 MHz to provide data transmission in NG-PON2 and new Super-PON optical networks.

3.4. Development of the Experimental 100 Gbit/s Data Centre Interconnect Based on a Micro-rod OFC Light Source

To meet the increasing bandwidth demand, data centre interconnects (DCIs) must offer higher performance and throughput while at the same time improving spectral efficiency and reducing power consumption [55]. IM-DD remains a promising DCI solution due to its low latency, high reliability, and reasonable cost [56].

The experimental up to 100 Gbit/s/λ data centre interconnect scheme is shown in Fig. 3.12.

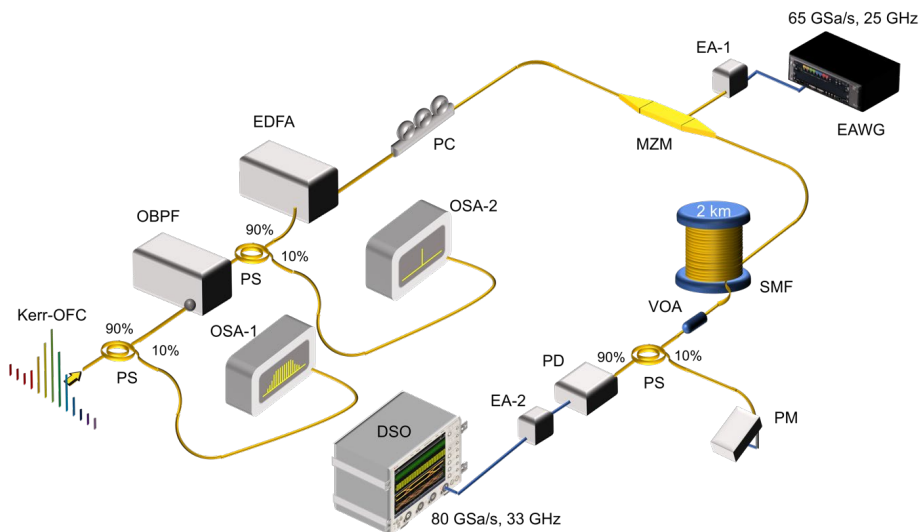


Fig. 3.12. An experimental high-speed optical interconnect scheme up to 100 Gbit/s/λ based on a micro-rod OFC light source.

The carriers (0) to (+6) of the micro-rod-based OFC light source are used to demonstrate the transmission of 50 Gbaud and 60 Gbaud NRZ-OOK and 50 Gbaud PAM-4 modulated signals over a 2 km long SMF line. The resulting OFC carrier signals are first sent to the OBPF (*Santec OTF-350*), which has a bandwidth of 35 GHz at the 3 dB level to separate one optical carrier at a time. PS with a ratio of 10/90 before and after OBPF have been used to capture the OFC spectrum with OSA-1 and a filtered OFC carrier with OSA-2, respectively. Then, the EDFA (*Amonics AEDFA-CL-18-B-FA*) with a fixed optical output power of 23.5 dBm amplifies the pre-filtered optical carriers before they are sent to the MZM (*Photline MX-LN40*), which has a bandwidth of 40 GHz at the 3 dB level, an extinction ratio of 20 dB, and an attenuation of 9 dB. The PC is placed before the MZM to reduce polarisation-dependent

attenuation. At this point in the circuit (before the MZM), the measured optical carrier signal power is around 5 dBm to ensure optimal optical power for data modulation.

High-speed NRZ-OOK and PAM-4 signals are first digitally generated using PRBS with a length of $2^{15}-1$. The signal is sampled and filtered using a raised cosine filter with a roll-off factor 1. This value is chosen because, with a lower roll-off factor, clock recovery does not work here due to stability fluctuations of individual optical carriers. The resulting signal is then loaded into an electrical arbitrary waveform generator (EAWG, *Keysight M9502A*, 25 GHz). In addition, frequency domain pre-equalisation up to 30 GHz bandwidth is applied to compensate for amplitude-frequency distortions and the limited bandwidth of the 65 GSa/s EAWG. Given these equipment limitations (65 GSa/s AWG is only 25 GHz bandwidth), maximum symbol rates of 50 Gbaud and 60 Gbaud have been chosen. In addition, it is assumed that if a 60 Gbaud symbol rate is possible with a given OFC, it provides performance tolerance for 40 Gbaud, which is more widely used at 100 GHz channel spacing. The generated output electrical signal is amplified by an electrical amplifier (EA-1, 38 GHz, 29 dB gain) and fed to the MZM. The modulated optical signal is then transmitted on a 2 km-long SMF line that further passes through the VOA. To control the optical power of the receiver, a PS with a ratio of 10/90 and a power meter (PM) are used. A high-power 50 GHz bandwidth InGaAs PIN photodetector (*Lab Buddy, DSC10H-39*) with +4 dBm sensitivity at $BER 10^{-12}$ and responsivity of 0.5 A/W is used to convert the received optical signal into an electrical signal. EA-2 (25 GHz, 16 dB gain) amplifies the electrical signal, and finally, DSO (*Keysight DSAZ334A*, 80 GSa/s, 33 GHz) samples the signal for further digital signal processing (DSP).

The received and sampled signal is processed using a DSP routine consisting of an LPF with a normalised bandwidth of 1.2, which provides optimal BER performance (Fig. 3.13), clock recovery, post-equalisation and a BER counter. LPF equalisation and a raised cosine filter have been applied with the aim of optimising the achieved performance of the transmitted signals.

In addition to the DSP functions mentioned above, adaptive equalisation (EQ) is also used to improve the quality of the received signal, namely to compensate for inter-symbol interference and the limited bandwidth of electrical components. EQ is performed by a decision feedback equalisation algorithm with 15 feed-forward taps (FFT) and 7 feedback taps (FBT) for 50 and 60 Gbaud NRZ-OOK transmission. However, the number of FFT and FBT used for the transmission of 50 Gbaud PAM-4 for each optical carrier channel is different – (0, +4, +5 – 55 FFT and 15 FBT; +1 – 85 FFT and 55 FBT; +2 – 23 FFT and 16 FBT; +3 – 10 FFT and 11 FBT). The number of taps chosen maximises the BER performance. In total, 1.2 million bits are used to calculate the BER .

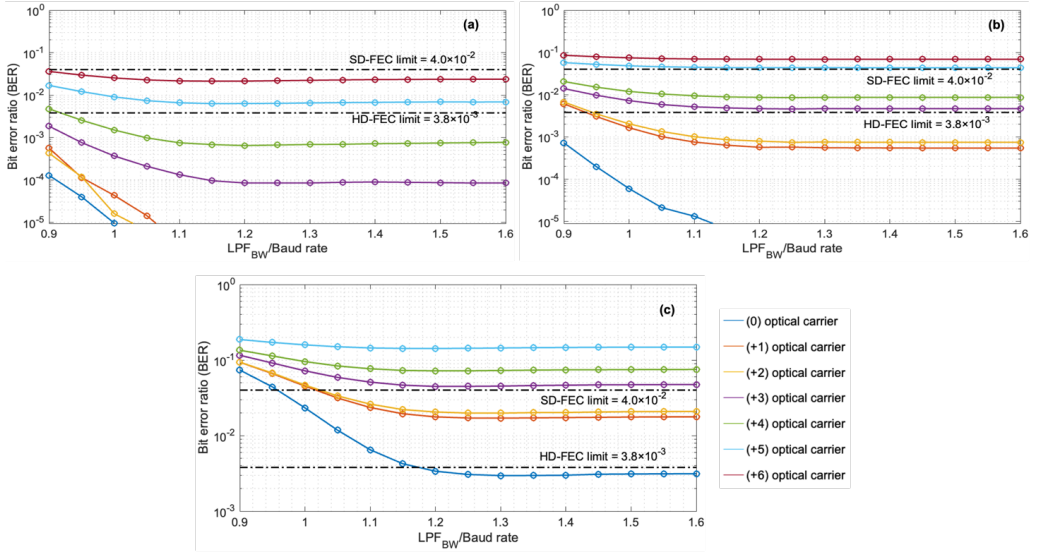


Fig. 3.13. *BER* compared to a normalised $LPF_{BW}/Baud$ relation IM/DD for a short-range optical DCI system with an applied OFC light source. In terms of *BER* performance, the worst-performing optical carrier (+6) provides transmission with a normalised LPF_{BW} bandwidth value of 1.2 for NRZ-OOK modulated signals at (a) 50 Gbaud/λ, (b) 60 Gbaud/λ, and (c) 50 Gbaud/λ for PAM-4 modulated signals.

Two *BER* threshold values are used in the quality analysis of the received NRZ-OOK and PAM-4 signals – HD-FEC with 7 % overhead and *BER* threshold of 3.8×10^{-3} , and soft-decision forward error correction (SD-FEC) with 20 % overhead and *BER* threshold of 4.0×10^{-2} . Data transmission is considered successful if the *BER* value of the received signal is below the given threshold values. The resulting 50 and 60 Gbaud NRZ-OOK data transmission results after 2 km transmission over the SMF line are shown both without and with EQ in Figs. 3.14 (a)–(d), whereas the 50 Gbaud PAM-4 transmission results are depicted in Figs. 3.14 (e)–(f).

In Fig. 3.14, different trends of *BER* curves can be observed for each optical carrier signal, even though the power of the optical carriers is amplified by the EDFA to one fixed power level before data modulation. This is explained by the fact that each carrier has a different OSNR value, which is the sum of two ASE noise-generating components – the EDFA in the OFC light source and the EDFA in the data transmission scheme. Consequently, the noise level increases significantly, which leads to reduced OSNR values of the optical carriers—Subsequently, the *BER* values of the received signal increase.

As seen in Fig. 3.14 (a), without EQ 50 Gbaud NRZ-OOK signal transmission is possible for OFC light source carriers from (0) at $\lambda = 1555.46$ nm to (+6) at $\lambda = 1559.78$ nm. The worst-performing data channel (based on *BER* value) is the carrier (+6), where the 20 % SD-FEC *BER* threshold is reached at -18 dBm received optical power. The best performance is shown with the optical carrier (0) – CW pumping source, which has the highest OFC light source output

optical power of +4 dBm and the highest TNR value of 52.8 dB. The 50 Gbaud NRZ-OOK signal transmission below 7 % HD-FEC threshold of 3.8×10^{-3} , is possible without EQ for OFC light source carriers (0) at $\lambda = 1555.46$ nm to (+4) at $\lambda = 1558.34$ nm. As one can see in Fig 3.14 (b), EQ slightly improves the BER performance compared to the previous case without EQ and enables 50 Gbaud NRZ-OOK signal transmission using carriers from (0) at $\lambda = 1555.46$ nm up to (+6) at $\lambda = 1559.78$ nm below the 20 % SD-FEC threshold value.

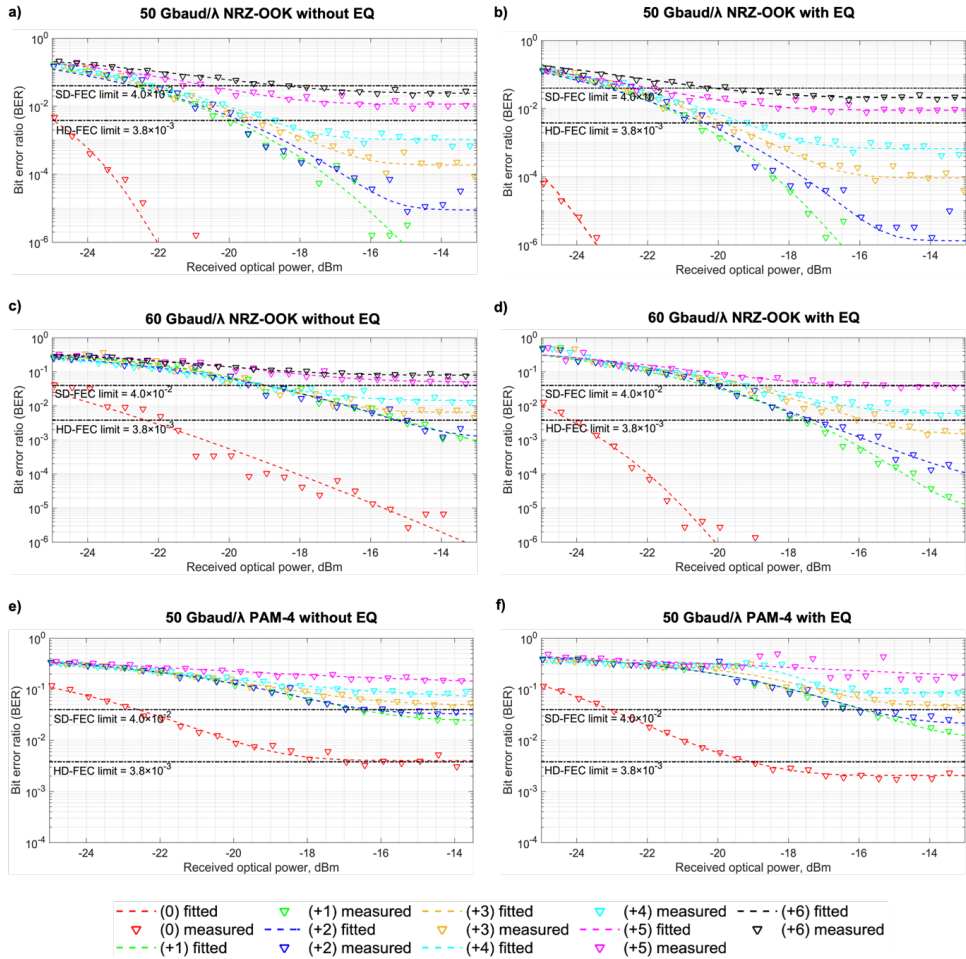


Fig. 3.14. BER correlation plots versus received optical power for IM/DD short-reach optical DCI system with applied OFC light source with NRZ-OOK at 50 Gbaud/λ (a) without and (b) with EQ, and at 60 Gbaud/λ (c) without and (d) with EQ. With PAM-4 at 50 Gbaud/λ (e) without and (f) with EQ. EQ for figures (b) and (d) uses 15 FFT and 7 FBT. EQ for figure (f) uses 55 FFT and 15 FBT in case of 0, +4; +5 carriers; 85 FFT and 55 FBT in case of +1; 23 FFT and 16 FBT in case of +2 and 10 FFT, and 11 FBT for the carrier +3.

As shown in Fig. 3.14 (c), without EQ 50, Gbaud NRZ-OOK signal transmission is possible by means of using carriers from (0) at $\lambda = 1555.46$ nm up to (+4) at $\lambda = 1558.34$ nm with the *BER* performance below the 20 % SD-FEC threshold level. The worst-performing data channel (based on *BER* value) is the carrier signal (+4), where the 20 % SD-FEC *BER* threshold is reached at -18 dBm received optical power. As in the previous case, also at 60 Gbaud NRZ-OOK, the highest quality data transmission is shown by the pumping carrier labelled (0). The results in Fig 3.14 (d) indicate that EQ significantly improves *BER* performance for 60 Gbaud NRZ-OOK signal transmission with carriers from (0) to (+5).

Without EQ, 50 Gbaud/ λ PAM-4 signal transmission can be realized using (0) carrier signal, which at -17 dBm received optical power ensures the *BER* value below 7 % HD-FEC threshold, refer to Fig. 3.14 (e). For carriers (+1) and (+2), *BER* values below the 20 % SD-FEC threshold are provided at -16 dBm received optical power. For other carriers, the *BER* of the received signal remains above the defined 20 % SD-FEC threshold. EQ improves performance by allowing transmission of a 50 Gbaud PAM-4 signal with (0) to (+2) carrier signals. In the case of EQ for optical carrier signals (0), *BER* is under 7 % HD-FEC threshold level 3.8×10^{-3} at -19 dBm of the received optical power, refer to Fig. 3.14 (f). However, for the optical carrier signals from (+1) to (+2), the minimum *BER* value is achieved under the 20 % SD-FEC threshold 4.0×10^{-2} at -16 dBm of the received optical power. Received eyelet/mesh diagrams for 50 Gbaud and 60 Gbaud NRZ-OOK and 50 Gbaud PAM-4 signals after 2 km transmission over SMF are shown for the (+1) carrier signal, refer to Fig. 3.15.

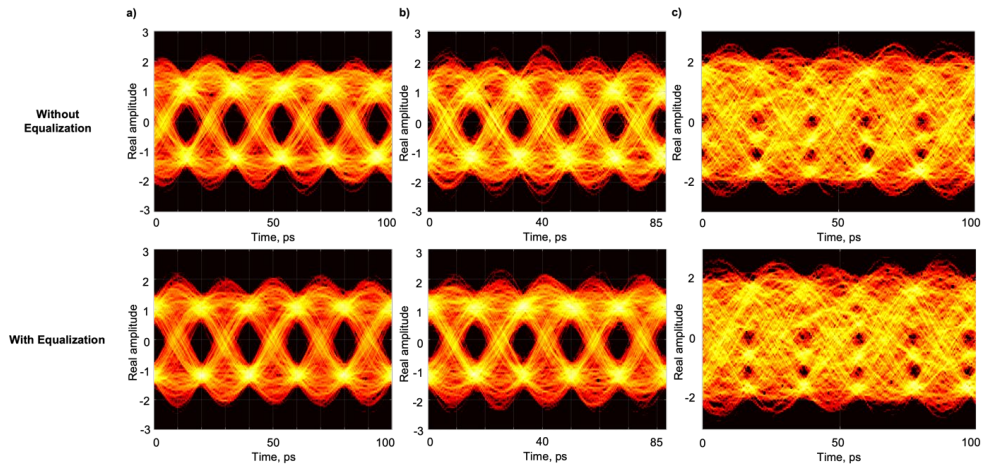


Fig. 3.15. Received signal eye diagrams with and without EQ for carrier (+1), captured at the received optical power of -12.5 dBm: for a) 50 Gbaud/ λ in the case of NRZ-OOK , b) 60 Gbaud/ λ in the case of NRZ-OOK, and c) 50 Gbaud/ λ in the case of PAM-4.

Summary

From the conducted research and obtained results, it can be concluded that the microsphere and micro-rod OFC light source can replace the optical carrier signals from the laser array in IM/DD WDM-PON and DCI systems. The obtained *BER* values are below those of HD-FEC and SD-FEC. OFC light source with microsphere resonator ($D = 328.5$ μm) can provide a

BER value of at least 9.1×10^{-4} in a 4-channel 200 GHz WDM-PON system with a transmission speed of 10 Gbit/s in a data channel at a 60 km transmission line. An OFC light source with a microsphere resonator ($D = 168 \mu\text{m}$) can provide a *BER* value of at least 2×10^{-5} ; 4.8×10^{-7} ; and 1×10^{-5} , at, respectively, 40 km long SMF, NZ-DSF, CSF transmission fibres in a 4-channel 393 GHz WDM-PON system with a data rate of 10 Gbit/s transmission. An OFC light source with a microsphere resonator ($D = 660 \mu\text{m}$) and the resulting soliton comb is able to provide a *BER* value of at least 2.7×10^{-12} ; 4.3×10^{-11} ; 3.2×10^{-11} ; and 1.2×10^{-6} for 100 kHz, 1 MHz, 10 MHz, and 100 MHz linewidth values of carriers in the 8-channel 100 GHz WDM-PON system with a data rate of 10 Gbit/s and a transmission line length of 50 km. Finally, an OFC light source with a micro-rod resonator ($D = 700 \mu\text{m}$) can achieve a *BER* value for carriers (0) to (+6) below the 20 % SD-FEC threshold at NRZ-OOK 50 Gbit/s transmission (by applying EQ), which for the (+6) carrier is achieved at -19.5 dBm received optical power. The NRZ-OOK 60 Gbit/s transmission on carriers (0) to (+5) below the 20 % SD-FEC threshold is achieved at -17 dBm received optical power for the (+5) carrier. The PAM-4 100 Gbit/s transmission on carriers (0) to (+2) below the 20 % SD-FEC threshold achieved at -16 dBm received optical power for the (+2) carrier. Original publications on the research described in this chapter can be found in **Appendices 1, 3, 4, and 6 of the Thesis.**

CONCLUSIONS

1. To develop microspheres with 175 μm and 350 μm diameters (Q -factor $\sim 10^7$) from 125 μm diameter SSMF, by means of a fibre splicer *Fujikura ARCMaster FSM-100P+*, takes 42 and 114 seconds, respectively; whereas, in order to develop, by means of a CO_2 laser, five 700 μm diameter micro-rods (Q -factor = 2.6×10^7) on one silica rod with 520 μm spacing between resonators, takes about 5 minutes.
2. In the developed WGM resonators, it is possible to obtain OFC in the optical C-band by pumping the resonators around the wavelength of 1550 nm, where the optimal gap between the TP and the resonator is 0.12 μm or 0.17 μm for light input into the resonator and choosing the diameter of the resonator allows to adjust the spacing between OFC carriers.
3. Based on the obtained experimental results, it can be concluded that OFC carriers corresponding to the inter-channel spacing defined in the ITU-T G.694.1 recommendation can be obtained by pumping the microsphere resonator ($D = 168 \mu\text{m}$) at 1558 nm wavelength with 16 dBm optical power – a spacing of 393 GHz is obtained, and pumping the micro-rod resonator from two sides ($D = 700 \mu\text{m}$; Q -factor = 2.6×10^7) at 1555.46 nm wavelength – a spacing of 90 GHz is acquired.
4. Based on the numerical results, it can be concluded that a soliton comb can be obtained with an OFC carrier signal spacing of 200 GHz by pumping a microsphere resonator ($D = 328.5 \mu\text{m}$) at a wavelength of 1552.52 nm as well as with an OFC carrier spacing of 100 GHz pumping a microsphere resonator ($D = \sim 660 \mu\text{m}$) at a wavelength of 1547.71 nm.
5. IM/DD for a WDM-PON system with 4 channels, 10 Gbit/s and 200 GHz inter-channel spacing of the received signal BER is 9.1×10^{-4} at a 60 km data line based on a microsphere OFC light source.
6. IM/DD for a WDM-PON system with 4 channels, 10 Gbit/s and 393 GHz inter-channel intervals of the received signal BER is 2×10^{-5} ; 4.8×10^{-7} ; and 1×10^{-5} at 40 km data transmission via SMF, NZ-DSF and CSF fibre lines, respectively, based on a microsphere OFC light source.
7. IM/DD for a WDM-PON system with 8 channels, 10 Gbit/s and 100 GHz inter-channel intervals of the received signal BER is 2.7×10^{-12} ; 4.3×10^{-11} ; 3.2×10^{-11} ; and 1.2×10^{-6} at 100 kHz, 1 MHz, 10 MHz, and 100 MHz carrier linewidths, respectively, over a 50 km transmission line based on a microsphere OFC light source.
8. For the IM/DD WDM DCI system, the worst BER channel achieves a 20 % SD-FEC threshold at -19.5 dBm and -17 dBm optical power with NRZ-OOK modulation at 50 Gbit/s and 60 Gbit/s, respectively, as well as at -16 dBm optical power with PAM-4 modulation at 100 Gbit/s based on a micro-rod OFC light source.

The results obtained during the research and presented in the Doctoral Thesis are presented in 6 original scientific articles, and in the proceedings of one scientific conference (indexed in Scopus, IEEE or Web of Science). In addition to the above, the results of the research are presented at 4 scientific conferences (not indexed in Scopus, IEEE or Web of Science).

REFERENCES

1. T. Bottger, G. Ibrahim, B. Vallis. How the Internet reacted to Covid-19 – A perspective from Facebook’s Edge Network, IMC’20, Oct. 27–29, Virtual Event, USA. 2020. DOI: doi.org/10.1145/3419394.3423621.
2. J. Malmodin and D. Lunden. The Energy and Carbon Footprint of the Global ICT and E&M Sectors 2010–2015, MDPI Sustainability, 10, 3027, 2018. DOI: doi.org/10.3390/su10093027.
3. C. Freitag, M. Berners-Lee, K. Widdicks, B. Knowles, G. S. Blair, and A. Friday. The real climate and transformative impact of ICT: A critique of estimates, trends, and regulations, Patterns, vol. 2, Iss. 9, 100340, Sept. 10, 2021. DOI: doi.org/10.1016/j.patter.2021.100340.
4. A. Jahid, S. Hossain, K. H. Monju, F. Rahman, and F. Hossain. Techno-Economic and Energy Efficiency Analysis of Optimal Power Supply Solutions for Green Cellular Base Stations, IEEE Access, vol. 8, 2020, pp. 43776–43795. DOI: doi.org/10.1109/ACCESS.2020.2973130.
5. A. S. Raja, S. Lange, M. Karpov, K. Shi, X. Fu, R. Behrendt, D. Cletheroe, A. Lukashchuk, I. Haller, F. Karinou, B. Thomsen, K. Jozwik, J. Liu, P. Costa, T. J. Kippenberg, and H. Ballani. Ultrafast optical circuit switching for data centers using integrated soliton microcombs, Nat. Commun., 12, art. no. 5867, 2021. DOI: doi.org/10.1038/s41467-021-25841-8.
6. Finisar Corporation, Product Specification, 100G 20km eLR4 QSFP28 Optical Transceiver Module (WDM-20), 2021, p. 7.
7. Eoptolink Technology Inc., Ltd., Product Specification, 100GBASE-SR10 100m CXP Optical Transceiver Module, 2014, p. 12.
8. ITU-T, Spectral grids for WDM applications: DWDM frequency grid (G.694.1), 2020, p. 16.
9. 40-Gigabit-Capable Passive Optical Networks 2 (NG-PON2: Physical Media Dependent (PMD) Layer Specification, document ITU-T Rec. G.989.2, International Telecommunication Union, Telecommunication Standardization Sector of ITU, 2019, pp. 1–114.
10. IEEE P802.3cs. Increased-reach Ethernet optical subscriber access (Super-PON) Task Force. Available online: <https://www.ieee802.org/3/cs/index.html>.
11. Lin. G., Diallo S., Chembo Y. K. Optical Kerr frequency combs: Towards versatile spectral ranges and applications, 2015 17th International Conference on Transparent Optical Networks (ICTON), Budapest, 2015, pp. 1–4. DOI: doi.org/10.1109/ICTON.2015.7193612.

12. Del'Haye, P. et al. Optical frequency comb generation from a monolithic microresonator, *Nature*, 450, 1214–1217, 2007. DOI: doi.org/10.1038/nature06401.
13. T. Tanabe, S. Fujii, and R. Suzuki. Review on microresonator frequency combs, *Jpn. J. Appl. Phys.*, vol. 58, art. no. SJ0801, July 2019. DOI: doi.org/10.7567/1347-4065/ab2aca.
14. Savchenkov A. A., Matsko A. B., Maleki L. On Frequency Combs in Monolithic Resonators, *Nanophotonics*, 5, 363–391 (2016). DOI: doi.org/10.1515/nanoph-2016-0031.
15. Pfeifle J., Lauermaun M., Wegner D., Brasch V., Herr T., Hartinger K., Li J., Hillerkuss D., Schmogrow R., Holtzwarth R., Freude W., Leuthold J., Kippenberg T. J., Koos C. Coherent terabit communications with microresonator Kerr frequency combs, *Nat. Photonics*, 8, 375 (2014). DOI: doi.org/10.1038/nphoton.2014.57.
16. P. Liao, C. Bao, A. Almainan, A. Kordts, M. Karpov, M. H. P. Pfeiffer, L. Zhang, F. Alishahi, Y. Cao, K. Zou, A. Fallahpour, A. N. Willner, M. Tur, T. J. Kippenberg and A. E. Willner. Demonstration of Multiple Kerr-Frequency-Comb Generation Using Different Lines from Another Kerr Comb Located Up To 50 km Away, *J. Light. Technol.*, vol. 37, 579 (2019). DOI: doi.org/10.1109/JLT.2019.2895851.
17. Lucas E., Jost J. D., Kippenberg T. J., Beha K., Lezius M., Holzwarth R. “Soliton-Based Optical Kerr frequency Comb for Low-Noise Microwave Generation”, Joint Conference of the European Frequency and Time Forum and IEEE International Frequency Control Symposium (EFTF/IFCS), Besancon, 2017, 9–13 July. DOI: doi.org/10.1109/FCS.2017.8088949.
18. Avino S., Giorgini A., Malara P., Gagliardi G., Natale P. D. Investigating the resonance spectrum of optical frequency combs in fiber-optic cavities, *Opt. Express*, 21, 13785 2013. DOI: doi.org/10.1364/OE.21.013785.
19. Pfeifle J. Terabit-Rate Transmission Using Optical Frequency Comb Sources, *Karlsruhe Series in Photonics & Communication*, 20, (2017).
20. Levy J. S., Gondarenko A., Foster M. A., Turner-Foster A. C., Gaeta A. L., Lipson M. CMOS-compatible multiple-wavelength oscillator for on-chip optical interconnects, *Nat. Photonics*, 4, 37, 2010. DOI: doi.org/10.1038/nphoton.2009.259.
21. Foster M. A., Levy J. S., Kuzucu O., Saha K., Lipson M., Gaeta A. L. Silicon-based monolithic optical frequency comb source, *Opt. Express*, 19, 14233, 2011. DOI: doi.org/10.1364/OE.19.014233.
22. Kurbatska I., Bobrovs V., Alevska A., Lyashuk I., Gegere L. “Spectral effective solutions for mixed line rate WDM-PON systems”, *Progress in Electromagnetics Research Symposium*, 2017, pp. 1771–1777. DOI: doi.org/10.1109/PIERS.2017.8262037.
23. Liopis O., Merrer P. H., Bouchier A., Saleh K., Cibiel G. “High-Q optical resonators: characterization and application to stabilization of lasers and high spectral purity oscillators”, *Proceeding of SPIE*, San Francisco, January 2010, p. 10. DOI: doi.org/10.1117/12.847164.

24. A. J. Maker, A. M. Armani. Fabrication of silica ultra high quality factor microresonators, *J. Vis. Exp.*, vol. 65, 2012, art. no. 4164. DOI: doi.org/10.3791/4164.
25. J. P. Laine, C. Tapalian, B. Little, H. Haus. Acceleration sensor based on high-Q optical microsphere resonator and pedestal antiresonant reflecting waveguide coupler, *Sens. Actuat. A-Phys.*, vol. 93, 2001, pp. 1–7. DOI: doi.org/10.1016/S0924-4247(01)00636-7.
26. K. Cognee. “Hybridization of open photonic resonators,” University of Amsterdam, University of Bordeaux, 2020.
27. L. D. Bino, J. M. Silver, M. T. M. Woodley, S. L. Stebbings, X. Zhao, and P. Del’Haye. Microresonator isolators and circulators based on the intrinsic nonreciprocity of the Kerr effect, *Optica*, vol. 5, no. 3, pp. 279–282, March 2018. DOI: doi.org/10.1364/OPTICA.5.000279.
28. Pasquazi, A., Peccianti, M., Razzari, L., et al. Micro-combs: A novel generation of optical sources. *Phys. Rep.* 2018, 729, 1– 81. DOI: doi.org/10.1016/j.physrep.2017.08.004.
29. Liang W., Matsko A. B., Savchenkov A. A., Ilchenko V. S., Seidel D., Maleki L. “Generation of Kerr Combs in MgF₂ and CaF₂ Microresonators”, 2011 Joint Conference of the IEEE International Frequency Control and the European Frequency and Time Forum (FCS) Proceedings, San Francisco, 2011. DOI: doi.org/ 10.1109/FCS.2011.5977756.
30. Anashkina E. A., Sorokin A. A., Marisova M. P., Andrianov A. V. Development and numerical simulation of spherical microresonators based on SiO₂ – GeO₂ germanosilicate glasses for generation of optical frequency combs, *Quantum Electron.*, 49, 371, 2019. DOI: doi.org/10.1070/QEL16963.
31. Song Z., Lei S., Linhao R., Yanjing Z., Bo J., Bowen X., Xinliang Z. Controllable Kerr and Raman-Kerr frequency combs in functionalized microsphere resonators, *Nanophotonics*, 8, 2321, 2019. DOI: doi.org/10.1515/nanoph-2019-0342.
32. Savchenkov A. A., Matsko A. B., Ilchenko V.S., Solomatine I., Seidel D., Maleki L. Tunable Optical Frequency Comb with a Crystalline Whispering Gallery Mode Resonator. *Phys. Rev. Lett.*, 101, 093902, 2008. DOI: doi.org/ 10.1103/PhysRevLett.101.093902.
33. I. S. Grudinin, N. Yu, and L. Maleki. Generation of optical frequency combs with a CaF₂ resonator, *Opt. Lett.*, vol. 34, no. 7, April 1, 2009. DOI: doi.org/10.1364/OL.34.000878.
34. Kippenberg, T. J., et.al. Dissipative Kerr solitons in optical microresonators, *Science*, 361, eaan8083, 2018. DOI: doi.org/10.1126/science.aan8083.
35. Bogaerts W., De Heyn P., Vaerenbergh T. V., De Vos K., Selvaraja S. K., Claes T., Dumon P., Bienstman P., Van Thorhout D., Baets R. Silicon microring resonators, *Laser Photonics Rev.*, 6, 47, 2012. DOI: doi.org/10.1002/lpor.201100017.
36. Agha I. H., Okawachi Y., Gaeta A. L. Theoretical and experimental investigation of broadband cascaded four-wave mixing in high-Q microspheres, *Opt. Express*, 17, 16209, 2009. DOI: doi.org/10.1364/OE.17.016209.

37. Fuji, S., Tanabe, T. Dispersion engineering and measurement of whispering gallery mode microresonator for Kerr frequency comb generation, *Nanophotonics*, 9(5), 2019-0497 2020. DOI: doi.org/10.1515/nanoph-2019-0497.
38. Demirtzioglou I., Lacava C., Bottrill K. R. H., Thomson D. J., Reed G. T., Richardson D. J., Petropoulos P. Frequency comb generation in a silicon ring resonator modulator, *Opt. Express*, 26, 790, 2018. DOI: doi.org/10.1364/OE.26.000790.
39. E. A. Anashkina, M. P. Marisova, A. V. Andrianov, R. A. Akhmedzhanov, R. Murnieks, M. D. Tokman, L. Skladova, I. V. Oladyshkin, T. Salgals, I. Lyashuk, A. Sorokin, S. Spolitis, G. Leuchs, and V. Bobrovs, Microsphere-based optical frequency comb generator for 200 GHz spaced WDM data transmission system, *Photonics*, vol. 7, no. 3, Sep. 2020, Art. no. 72. DOI: doi.org/10.3390/photonics7030072.
40. Fülöp, A. Mazur, M. Lorences-Riesgo, A. Helgason, Ó. B. Wang, P. H. Xuan, Y. Leaird, D. E. Qi, M. Andrekson, P.A. Weiner, A.M. Torres-Company, V. High-order coherent communications using mode-locked dark-pulse Kerr combs from microresonators. *Nat. Commun.* 2018, 9, 1598. DOI: doi.org/10.1038/s41467-018-04046-6.
41. Wang, Y. Anderson, M. Coen, S. Murdoch, S. G. Erkintalo, M. Stimulated Raman scattering imposes fundamental limits to the duration and bandwidth of temporal cavity solitons. *Phys. Rev. Lett.* 2018, 120, 053902. DOI: doi.org/10.1103/PhysRevLett.120.053902.
42. Milián, C., Gorbach, A. V., Taki, M., Yulin, A. V., Skryabin, D. V. Solitons and frequency combs in silica microring resonators: Interplay of the Raman and higher-order dispersion effects. *Phys. Rev. A* 2015, 92, 033851. DOI: doi.org/10.1103/PhysRevA.92.033851.
43. Salgals, T., Alnis, J., Ozolins, O., Andrianov, A.V., Anashkina, E.A., Brice, I., Berkis, R., Pang, X., Udalcovs, A., Porins, J., Spolitis, S., Bobrovs, V. Silica Microsphere WGMR-Based Kerr-OFC Light Source and Its Application for High-Speed IM/DD Short-Reach Optical Interconnects. *Appl. Sci.* 2022, 12, 4722. DOI: doi.org/10.3390/app12094722
44. M. G. Suh and K. J. Vahala. Soliton microcomb range measurement, *Science*, vol. 359, Iss. 6378, pp. 848–887, 2018. DOI: doi.org/10.1126/science.aao1968.
45. D. C. Cole, E. S. Lamb, P. Del’Haye, S. A. Diddams, and S. B. Papp. Soliton crystals in Kerr resonators, *Nat. Photon.*, vol. 11, pp. 671–676, 2017. DOI: doi.org/10.1038/s41566-017-0009-z.
46. X. Xue, P. H. Wang, Y. Xuan, M. Qi, and A. M. Weiner. Microresonator Kerr frequency comb with high conversion efficiency, *Laser Photonics Rev.*, vol. 11, Iss. 1, art. no. 1600276, 2017. DOI: doi.org/10.1002/lpor.201600276.
47. A. Udalcovs, T. Salgals, L. Zhang, X. Pang, A. Djupsjöbacka, S. Spolitis, V. Bobrovs, S. Popov, and O. Ozolins. Optical Power Budget of 25+ Gbps IM/DD PON with Digital Signal Post-Equalization, *Appl. Sci.*, 10, 6106, 2020. DOI: doi.org/10.3390/app10176106.
48. IXblue Photonics “MX-LN series 1550 nm band Intensity Modulators,” Technical Specification, 1–6, 2019.

49. Characteristics of a Single-Mode Optical Fibre and Cable, document ITU- T Rec. G.652, International Telecommunication Union, Telecommunication Standardization Sector of ITU, 2016, pp. 1–17.
50. Characteristics of a Non-Zero Dispersion-Shifted Single-Mode Optical Fibre and Cable, document ITU-T Rec. G.655, International Telecommunication Union, Telecommunication Standardization Sector of ITU, 2009, pp. 1–17.
51. Characteristics of a Cut-Off Shifted Single-Mode Optical Fibre and Cable, document ITU-T Rec. G.654, International Telecommunication Union, Telecommunication Standardization Sector of ITU, 2020, pp. 1–16.
52. X. Pang, O. Ozolins, S. Gaiarin, M. I. Olmedo, R. Schatz, U. Westergren, D. Zibar, S. Popov, and G. Jacobsen, Evaluation of high-speed EML-based IM/DD links with PAM modulations and low-complexity equalization, ECOC, Dusseldorf, 2016, pp. 1–3.
53. M. W. Harrington, G. M. Brodnik, T. C. Briles, J. R. Stone, R. H. Streater, S. B. Papp, and D. J. Blumenthal. Kerr Soliton Microcomb Pumped by an Integrated SBS Laser for Ultra-Low Linewidth WDM Sources. Optical Fiber Communication Conference, San Diego, California USA, 8–12 March, 2020. DOI: doi.org/10.1364/OFC.2020.T4G.6.
54. Chan, C. C. K. Optical Performance Monitoring. Advanced Techniques for Next-Generation Photonic Networks. Elsevier: London, UK, 2010.
55. S. T. Ahmad, P. D. Lakshmijayasimha, A. K. Anandarajah, C. Browning, P. M. Anandarajah. Active Demultiplexer-enabled Directly Modulated DMT Transmission Using Optical Frequency Combs for Data Center Interconnects, *J. Light. Technol.* 39(17), 5468-5473 (2021). DOI: doi.org/10.1109/JLT.2021.3091959.
56. S. Fujii, S. Tanaka, T. Ohtsuka, S. Kogure, K. Wada, J. Kumazaki, S. Tasaka, Y. Hashimoto, Y. Kobayashi, T. Araki, K. Furusawa, N. Sekine, S. Kawanishi, and T. Tanabe, Dissipative Kerr soliton microcombs for FEC-free optical communications over 100 channels, *Opt. Express*, 30(2), 1351–1364, 2022. DOI: doi.org/10.1364/OE.447712.



Rihards Mūrnieks was born in 1996 in Jūrmala. He obtained a Bachelor's degree of Engineering Science in Electrical Science (2018) and a Master's degree of Engineering Science in Telecommunications (2020) from Riga Technical University (RTU). In 2018, he started working at RTU as a scientific assistant. Currently, he is a researcher and lecturer at RTU and, at the moment, has co-authored 13 scientific publications in industry-leading peer-reviewed journals and conferences. His research interests include, but are not limited to, optical frequency comb generation in non-linear microresonators, non-linear optics, optical access networks, and data-centre interconnects.

During his bachelor's studies, he was a member of the Electronics and Telecommunications Faculty Student's Council; in 2018, he was included in the RTU Golden Fund; and in 2022, he was awarded the acknowledgement of personal dedication to the development of RTU.